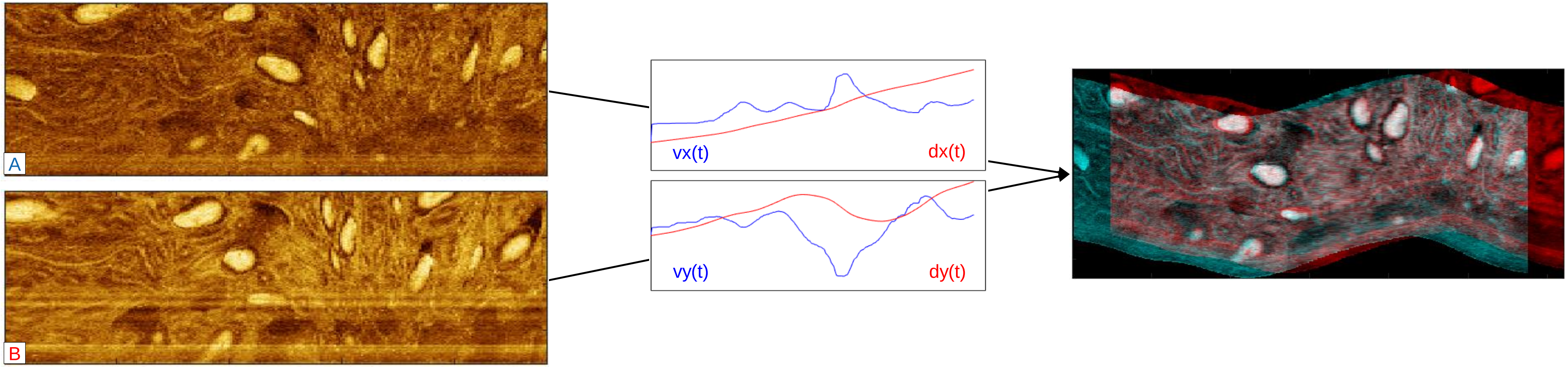

Dual-Beam Manually-Actuated Distortion Corrected Imaging:

2D scanning using single-axis galvanometer with automated distortion correction

Master Thesis

Madeline Harlow

Supervisors:

Prof. Dr. Markus Rudin (ETH)

Dr. Anthony Lee (BCCRC)

BC CANCER

Agenda

- Motivation
- DMDI and previous work
- Thesis Objective and Aims
  1. Optical Set up
  2. Acquire and Preprocess Images
  3. Calibration
  4. Automated Distortion Correction
  5. Validation and Testing
- Future Outlook

[1]

Motivation – Pitfalls in Optical Scanners

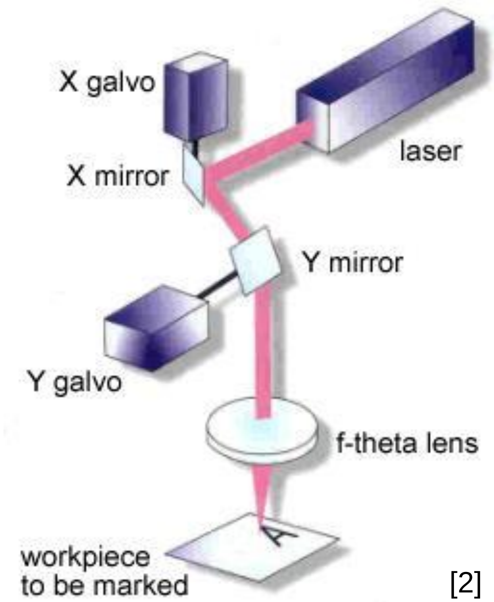

[2]

Galvanometer

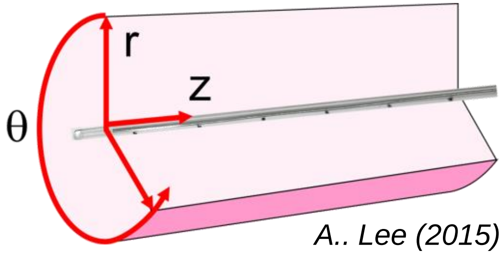

A.. Lee (2015)

Rotary (Catheter)

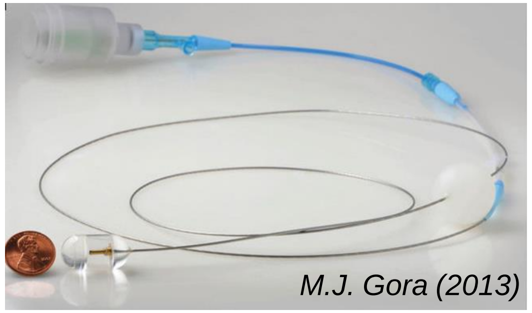

M.J. Gora (2013)

Rotary (Capsule)

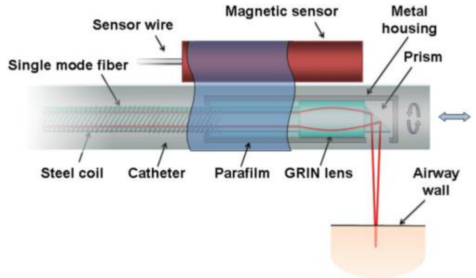

(Sensored) Magnetic Tracking

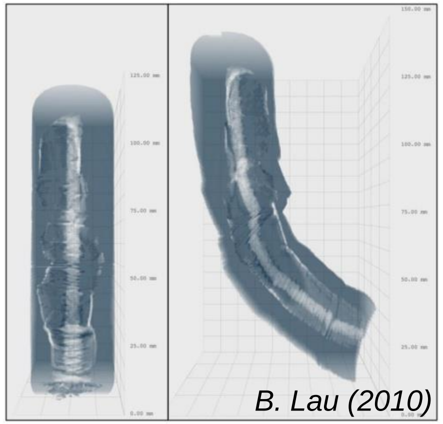

B. Lau (2010)

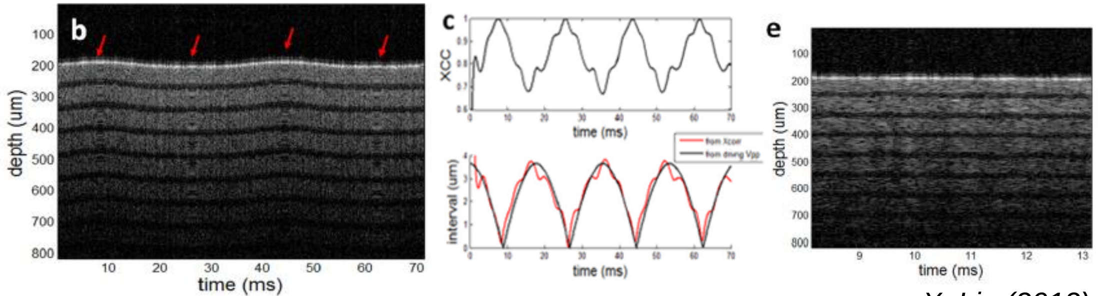

(Sensorless) Speckle Correlation

X. Liu (2012)

Disadvantage: **Small FOV**

- Mosaic – time consuming and stitching
- Motorized Pullback – length limited
- Manual Pullback – non-uniform motion distortion

Disadvantage: **Non-uniform motion distortion**

- Sensored – added hardware and complexity
- Sensorless – 2D extension not trivial

All are susceptible to **patient/clinician motion artefacts**

DMDI – Principle of Operation (in 1D)

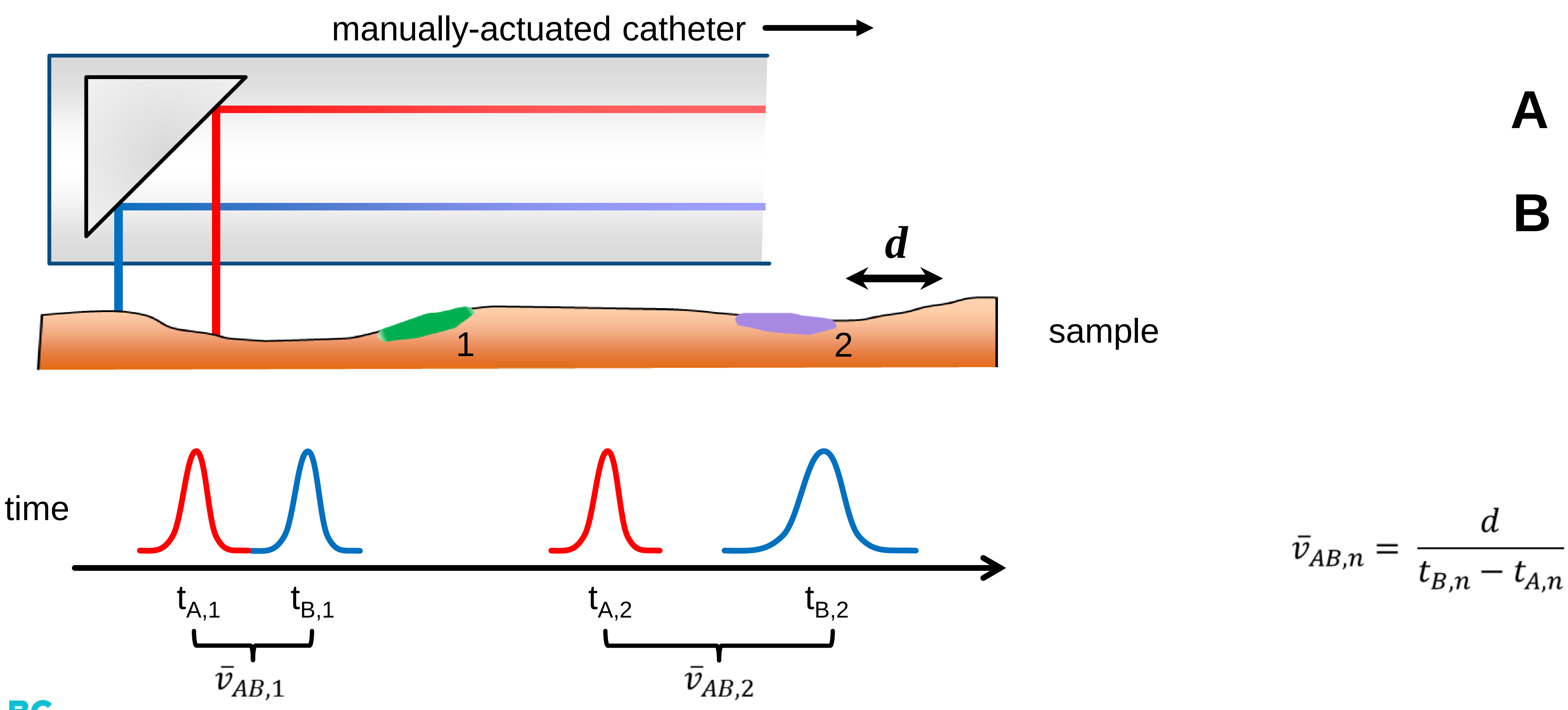

$$\bar{v}_{AB,n} = \frac{d}{t_{B,n} - t_{A,n}}$$

DMDI – First Implementation using DBMC

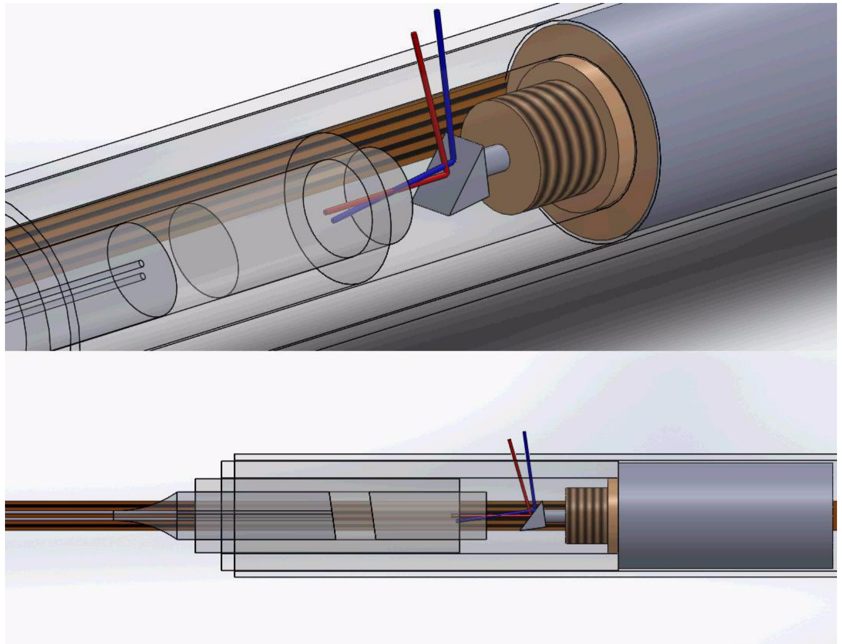

Dual-beam micromotor catheter (DBMC)

A. Lee (2017)

Manually actuated
en face OCT images

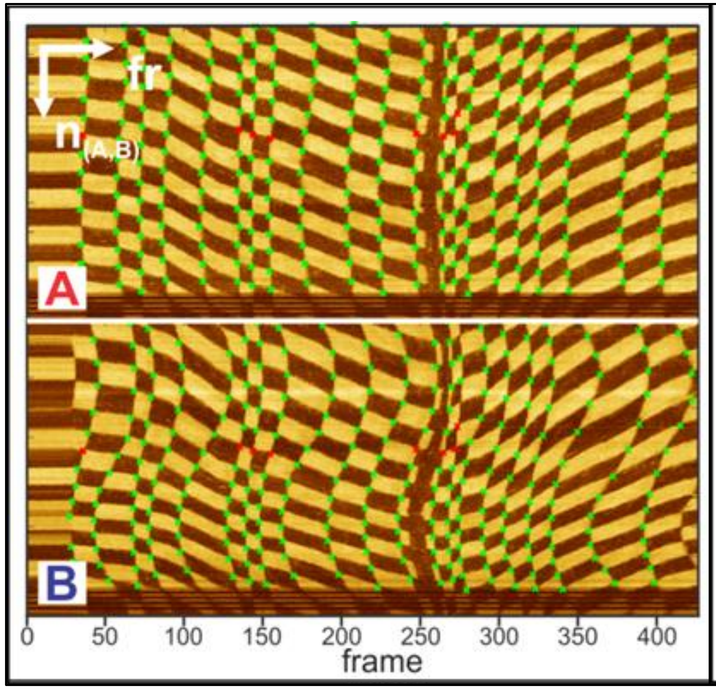

Manual control point selection

Distortion Corrected Images

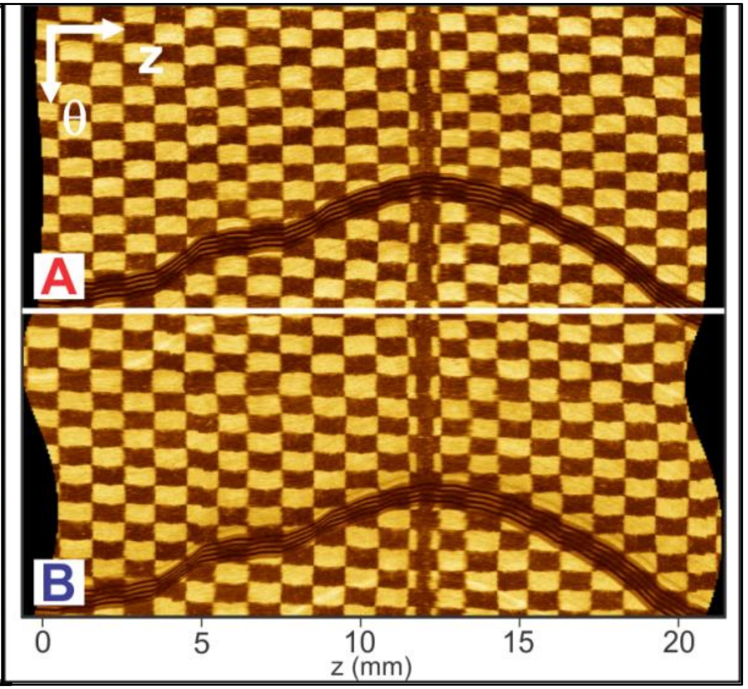

Thesis Objective

Develop DMDI to become more accessible and attractive for future clinical applications

- Investigate new implementation of DMDI
  - i.e. using a galvanometer
- Develop automated distortion correction

Thesis Aims

- Construct optical set up
- Establish image acquisition and preprocessing
- Calibrate to characterize the scanning pattern
- Develop automated distortion correction
- Validate and Test

DMDI Implemented using *en face* OCT Imaging

- Light analogy of ultrasound
  - Higher resolution (~ 1-10 µm)
  - But shorter penetration (~ 2 mm)
- Optical Coherence Tomography
  - O: near-infrared (900-1310 nm)
  - C: interferometry - compare coherent sample and reference arms to detect interference pattern
  - T: use consecutive scans to reconstruct
- *En face* imaging
  - Mean z (depth) projection of 3D OCT data
  - Creates 2D x-y slice image

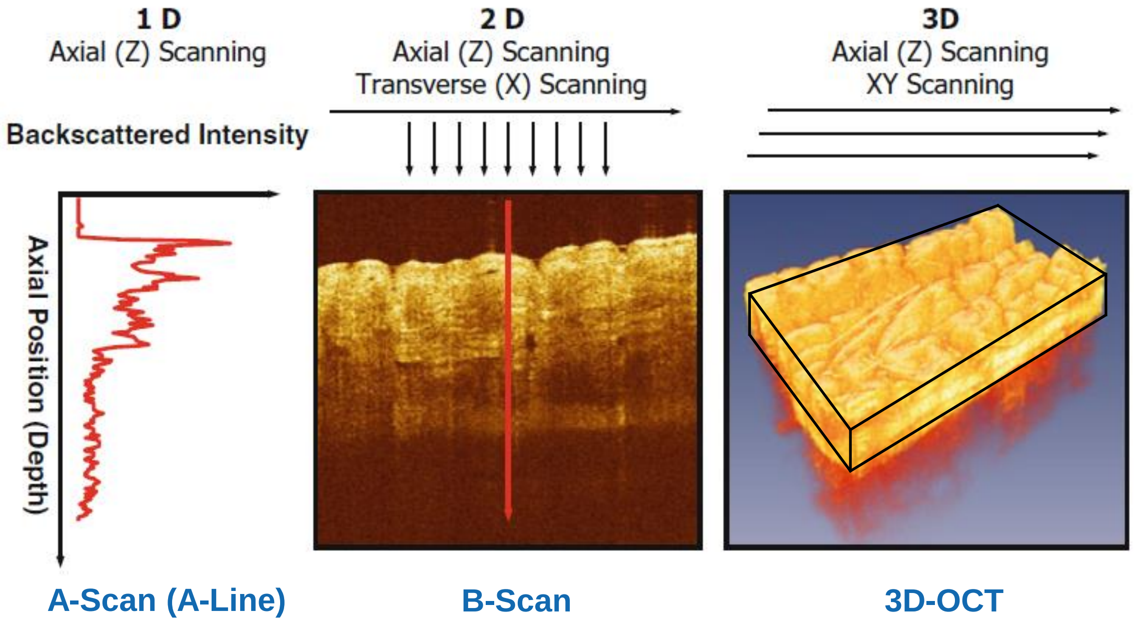

J.G. Fujimoto, W. Drexler (2015)

Optical Setup

- a) OCT Imaging System
  - Mach Zehnder Interferometer
  - Two channels
  - 100 kHz swept source (1310 nm)
- b) Galvanometer Imaging Head
  - DFP – dual pigtail fibre
  - GRIN – graded index lens
  - Two aligned and collimated beams
- c) Scan pattern
  - Calibrate to determine parameters
- d) Galvanometer waveform
  - Modified saw tooth

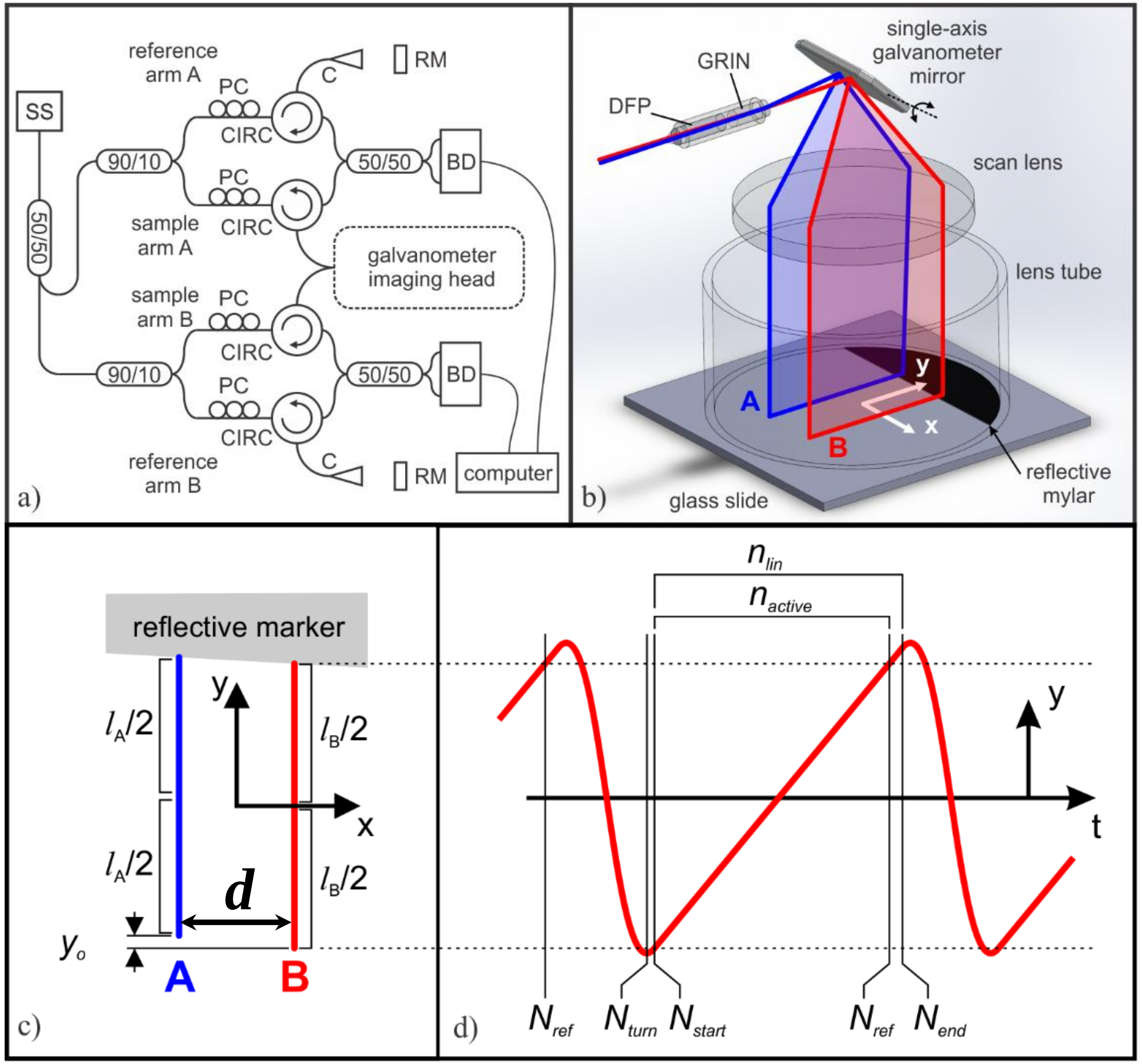

Image Acquisition

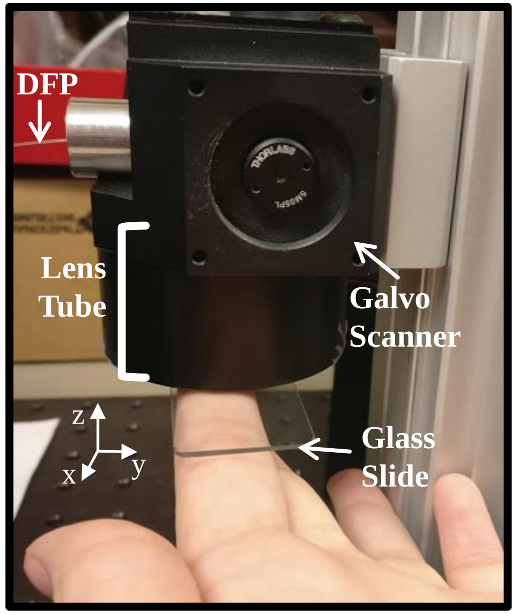

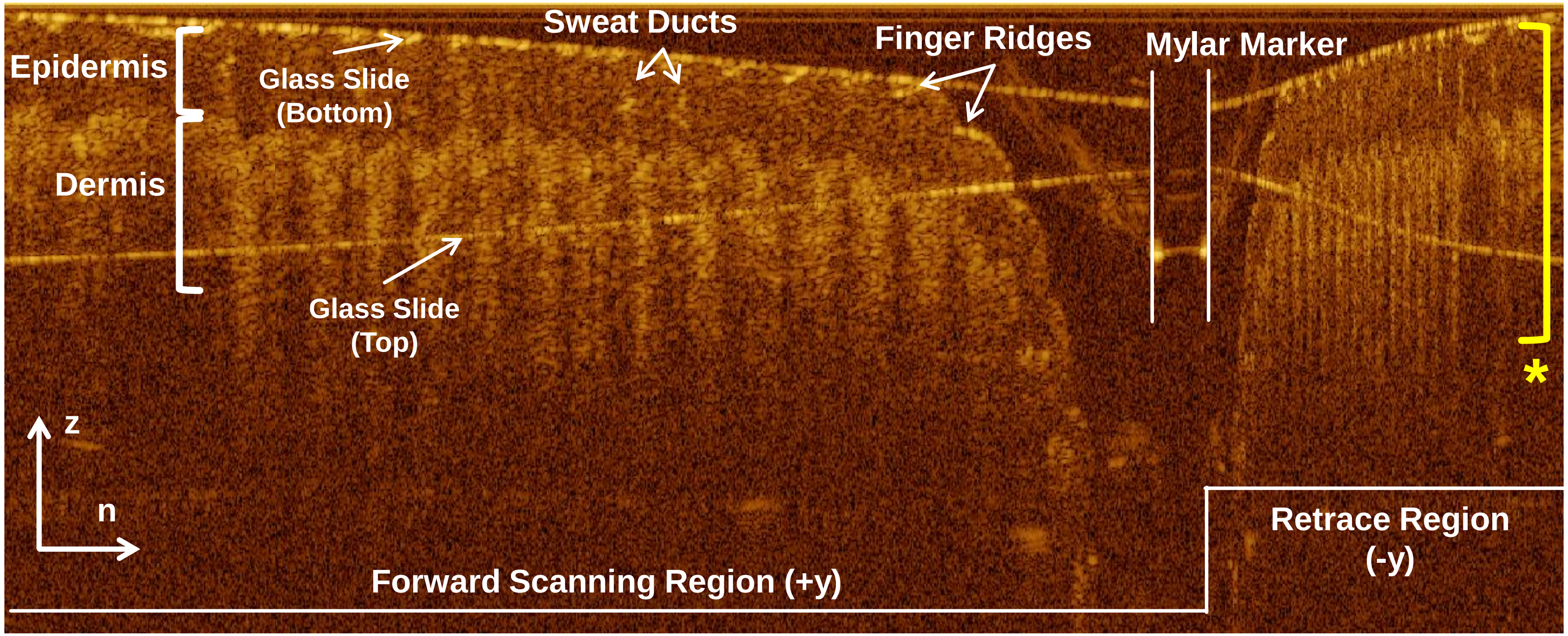

From Beam A
Manually Actuated Fingerprint

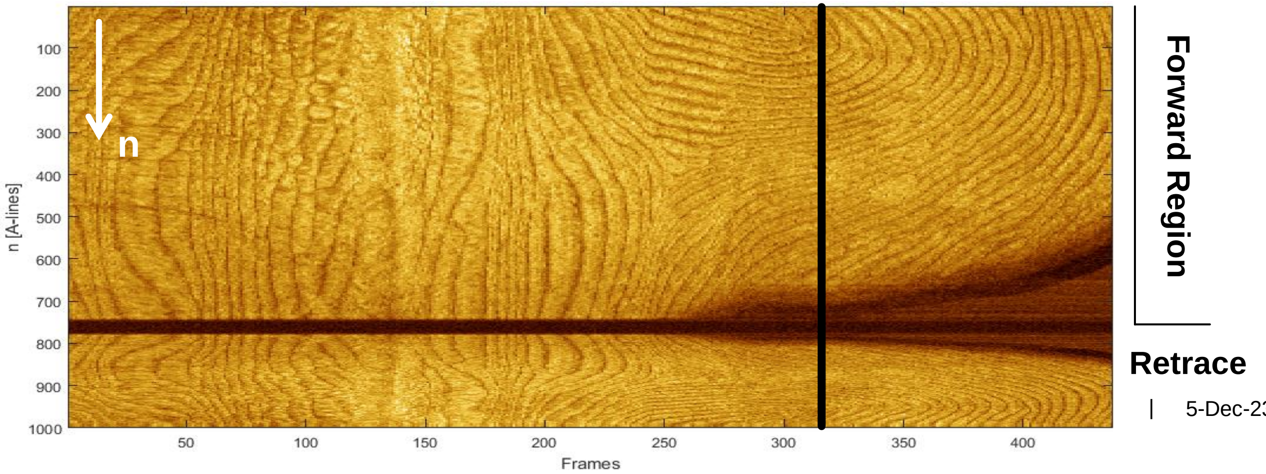

Image Preprocessing

From Beam B
Manually Actuated
QR code printed
paper phantom

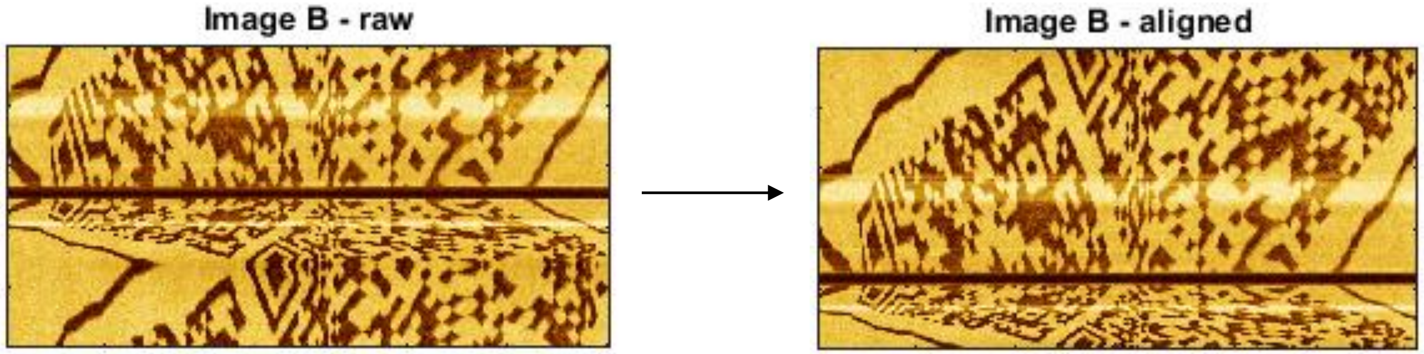

A
B

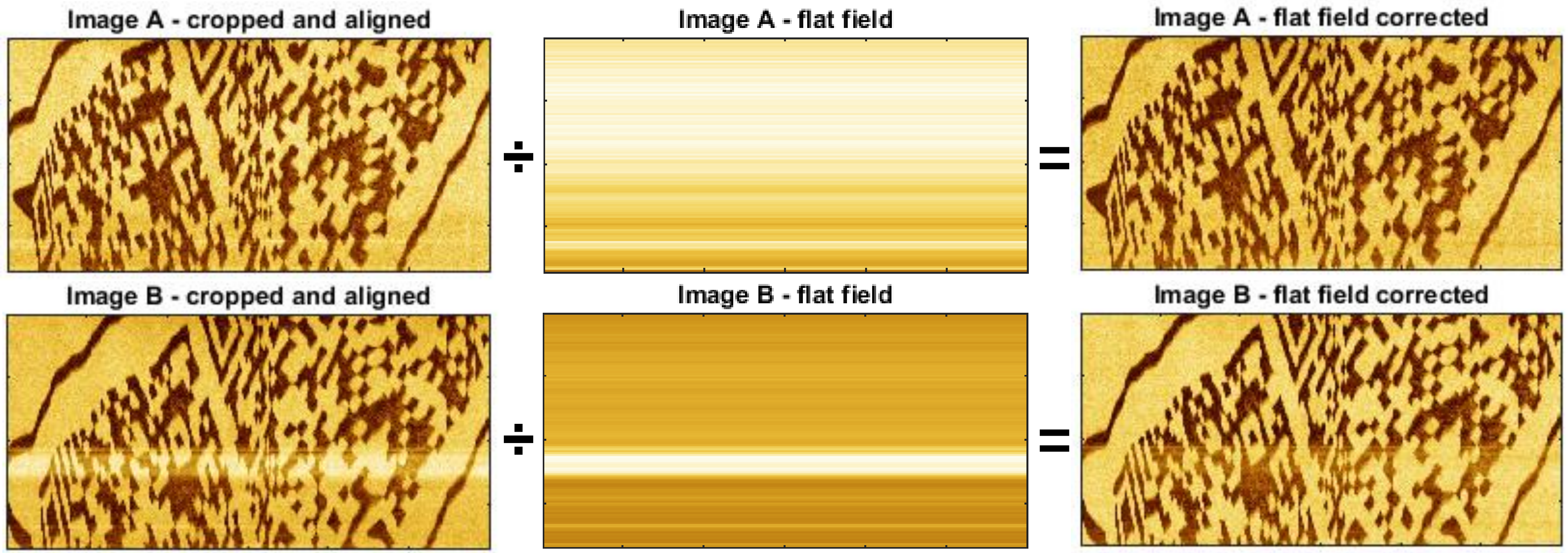

Calibration

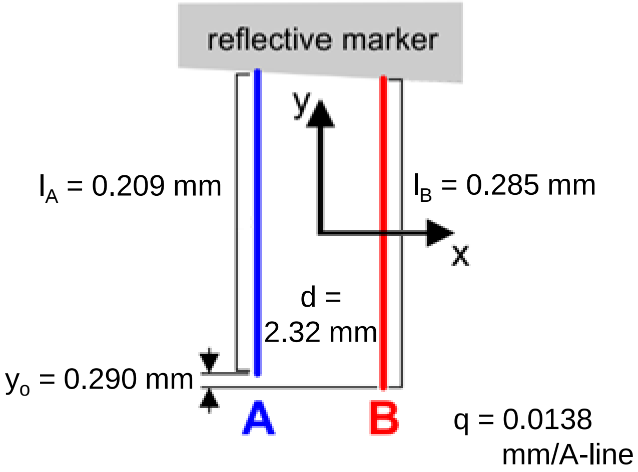

1. Stationary

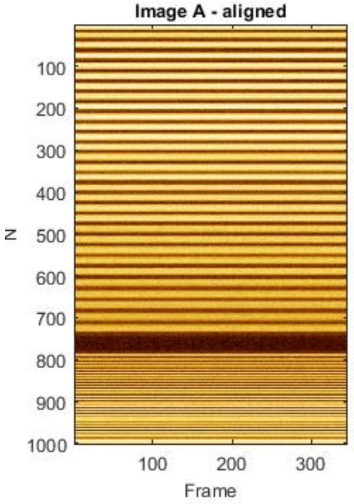

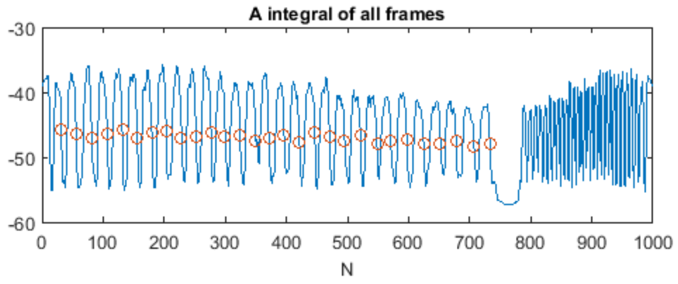

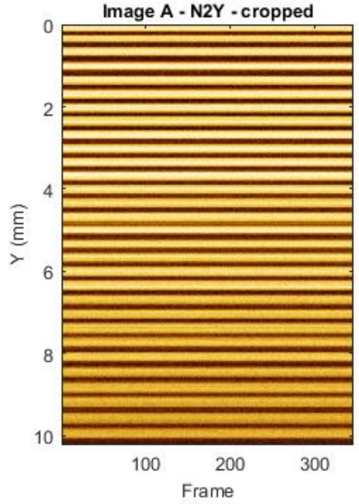

l_A = 10.209 mm
l_B = 10.285 mm

n → y

q = 0.0138
mm per A-line

2. Constant Motion

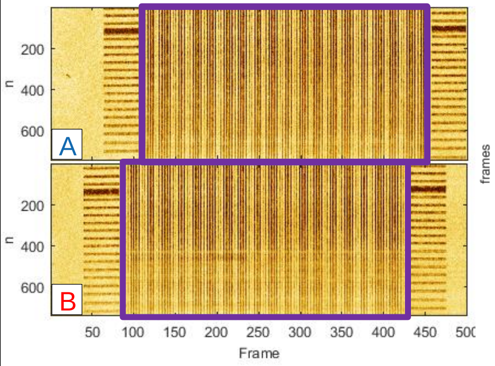

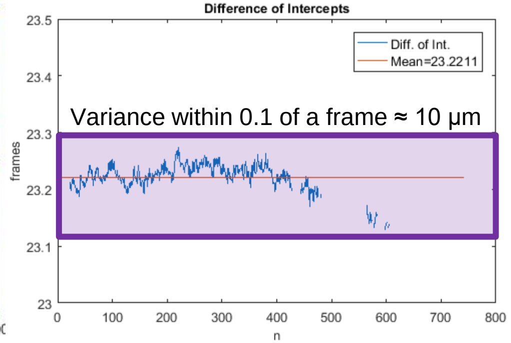

Assume parallel and straight lines
Scanline separation: **d = 23.2211 mm**

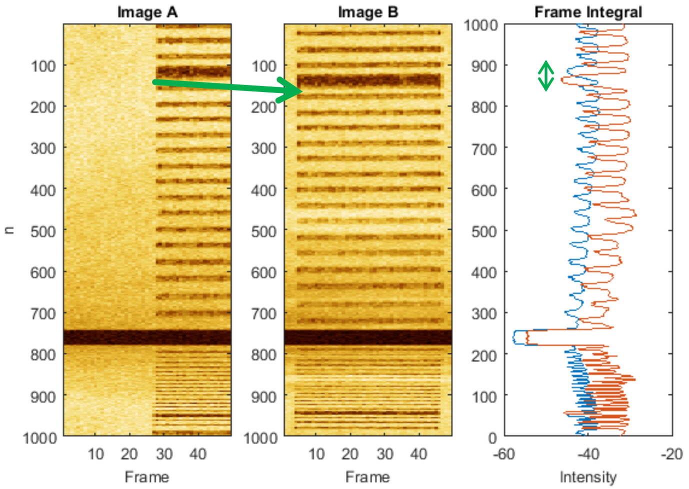

y_o = q * 21 A-lines = **0.290 mm**

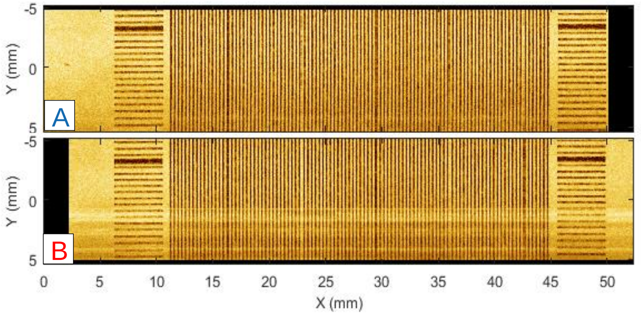

Corrected Images

Automated Distortion Correction

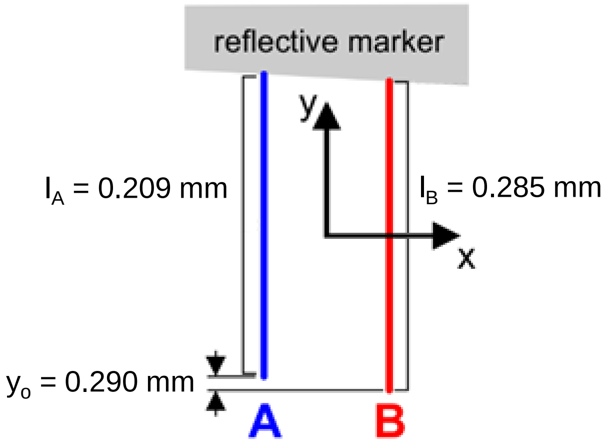

d = 2.32 mm
q = 0.0138 mm/A-line

$$x_A(t) = d_x(t) + \frac{d}{2}$$
$$y_A(t) = d_y(t) + q \cdot n_A(t) + y_o$$
$$x_B(t) = d_x(t) - \frac{d}{2}$$
$$y_B(t) = d_y(t) + q \cdot n_B(t)$$

- Pixels from distorted images can be mapped to generate corrected images using
  - Calibrated scanning pattern
  - Estimated velocity (displacement) profile
- To estimate velocity profile
  - Automated feature detection
  - Velocity estimate
  - Displacement calculation

Automated Feature Detection

$$\gamma(u,v) = \frac{\sum_{x,y}\left[f(x,y) - \bar{f}_{u,v}\right]\left[t(x-u,y-v) - \bar{t}\right]}{\left\{\sum_{x,y}\left[f(x,y) - \bar{f}_{u,v}\right]^2 \sum_{x,y}\left[t(x-u,y-v) - \bar{t}\right]^2\right\}^{0.5}}$$

Normalized Cross Correlation
(MATLAB normxcorr2)
f is the image, *t* is the mean template
$f_{u,v}$ is the mean *f* under the template

Preprocessed Images

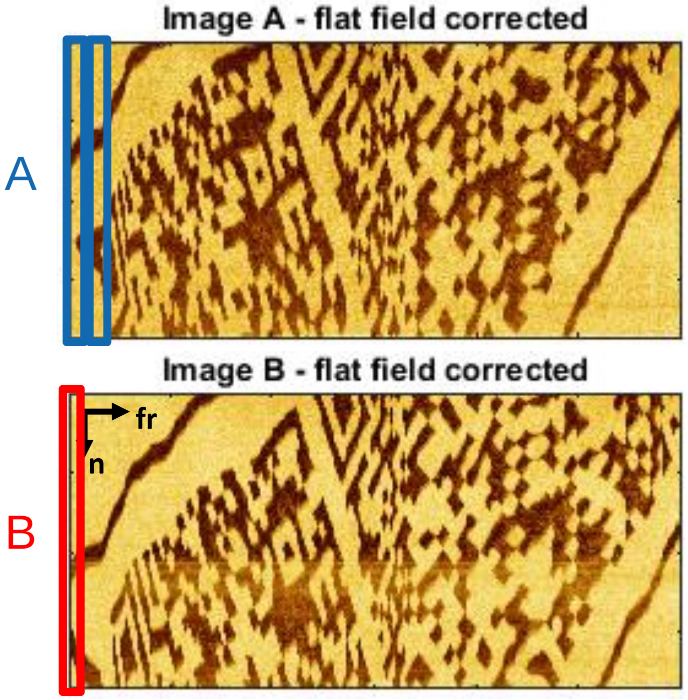

3D Correlation Coefficient Matrix

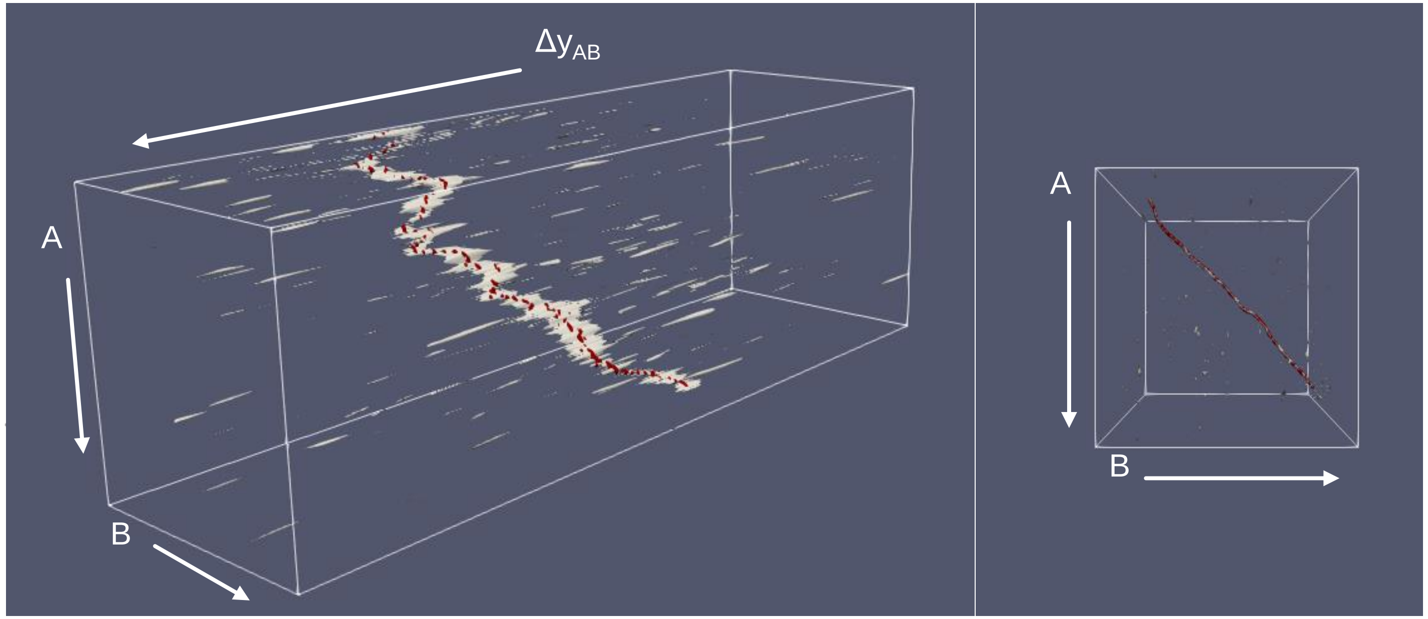

Pathway represents frame/frame/Δy combinations
with high correlation → Likely a matching feature

Automated Feature Detection

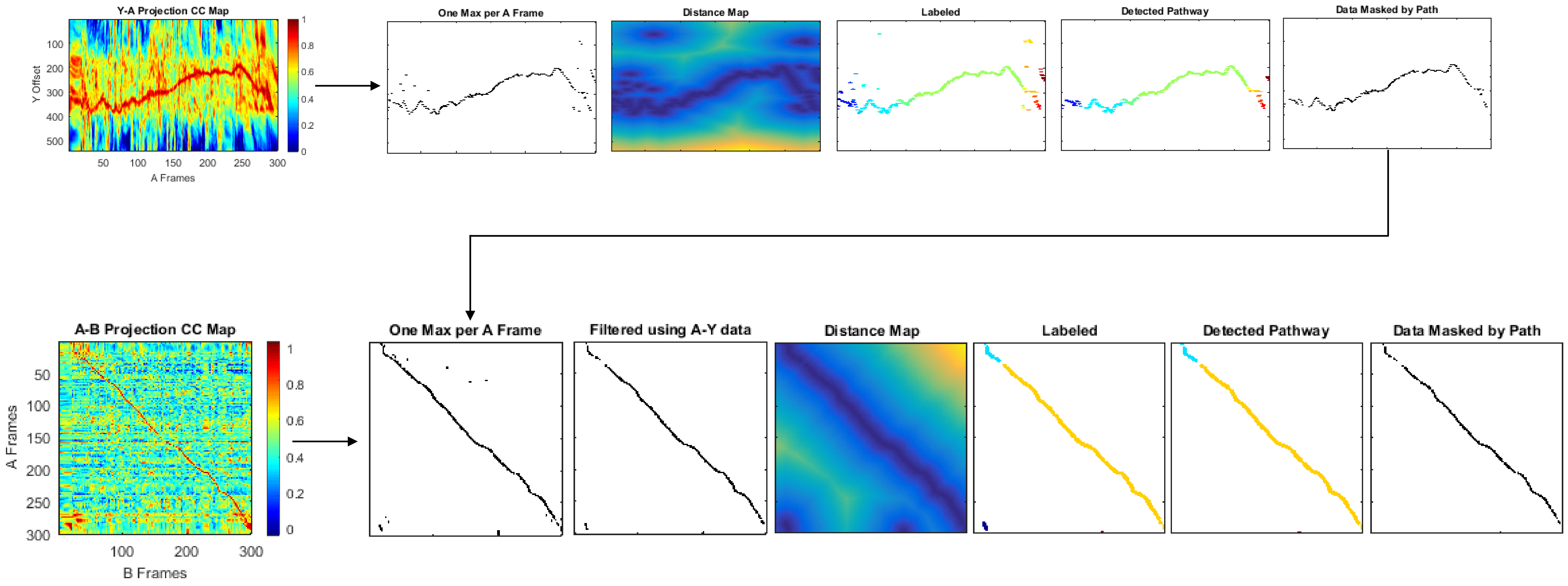

Velocity Profile Estimation

Average velocities per matching feature k

$$t_{AB,k} = \frac{(fr_{B,k} - fr_{A,k})}{f_{fr}} \qquad \bar{v}_{x,k} = \frac{d}{t_{B,k} - t_{A,k}} \qquad \bar{v}_{y,k} = \frac{q(\Delta y_{AB,k} - \Delta y_o)}{t_{B,k} - t_{A,k}}$$

k *is the feature matching pair index*
$fr_{AB,K}$ *is the A or B frame index at k*
f_{fr} *is the frame rate* $= 100\ fr/s$
$\Delta y_{AB,k}$ *is the y displacement at k*
Δy_o *is the zero displacement index*

Estimated weighted instantaneous velocities

$$v_{(x,y)}(t) \approx \frac{\sum_k \left(\bar{v}_{(x,y),AB,k} \cdot w_k(t)\right)}{\sum_k w_k(t)}$$

$$w_k(t) = \begin{cases} \dfrac{1}{t_{B,k} - t_{A,k} + 1}, & t \in [t_{A,k}, t_{B,k}] \\ 0, & elsewhere \end{cases} \qquad \left(\sum_{t=t_{A,k}}^{t_{B,k}} w_k(t) = 1\right)$$

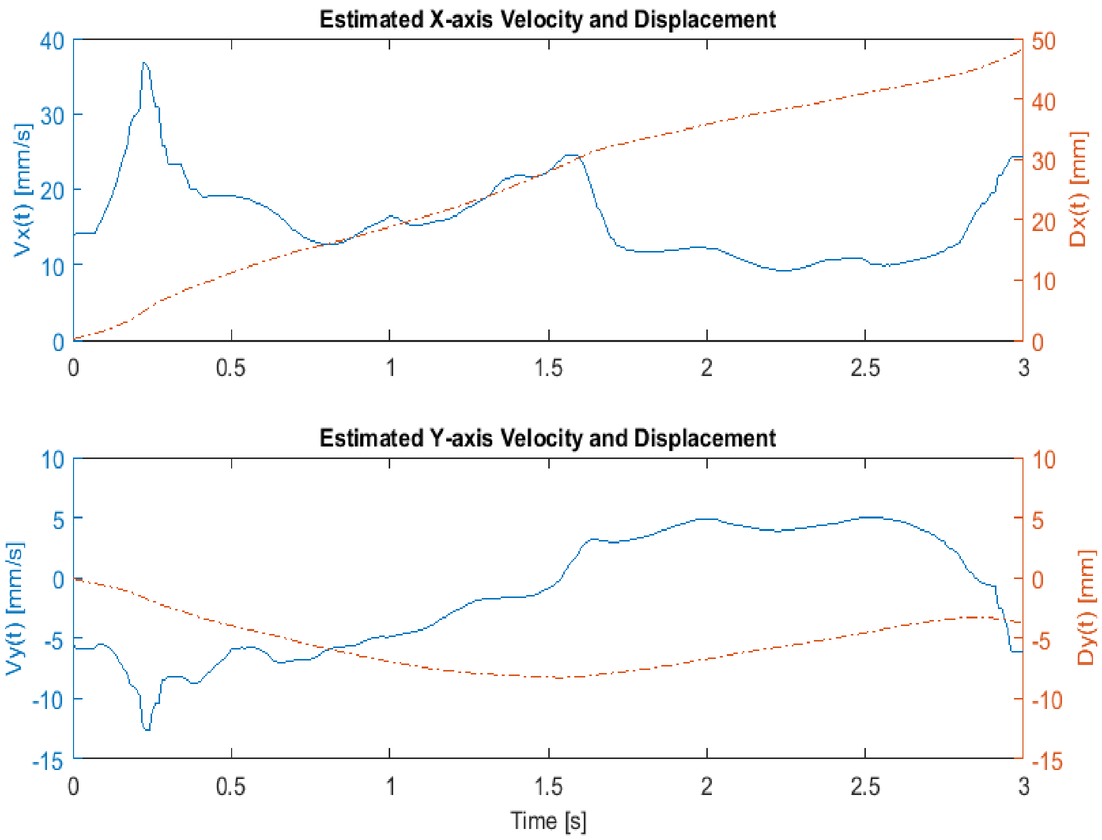

Generate Distortion Corrected Images

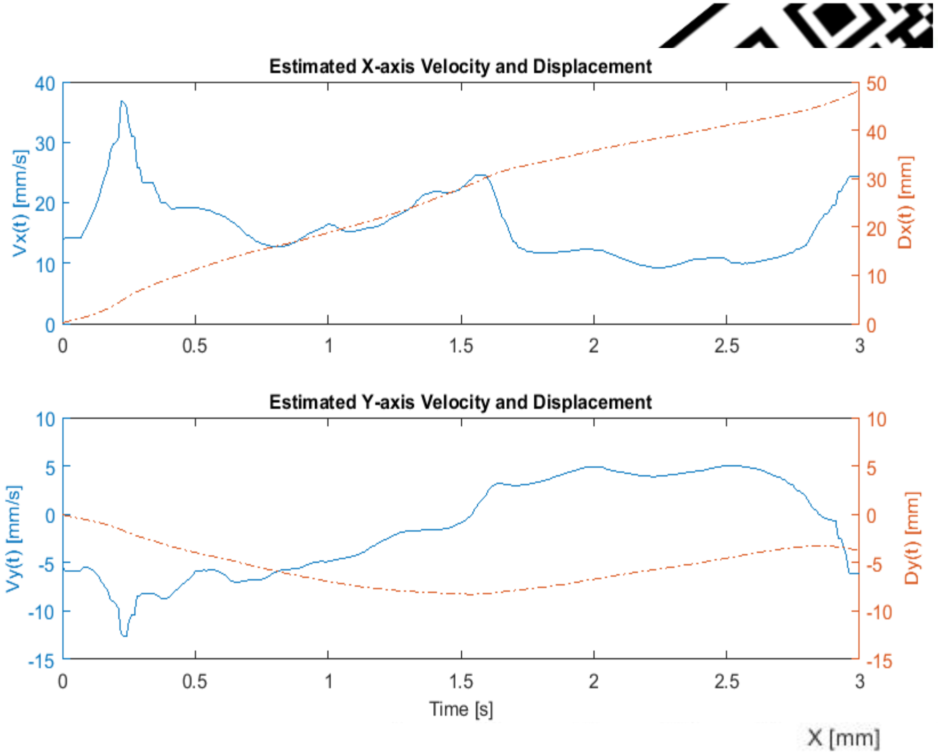

Preprocessed Images

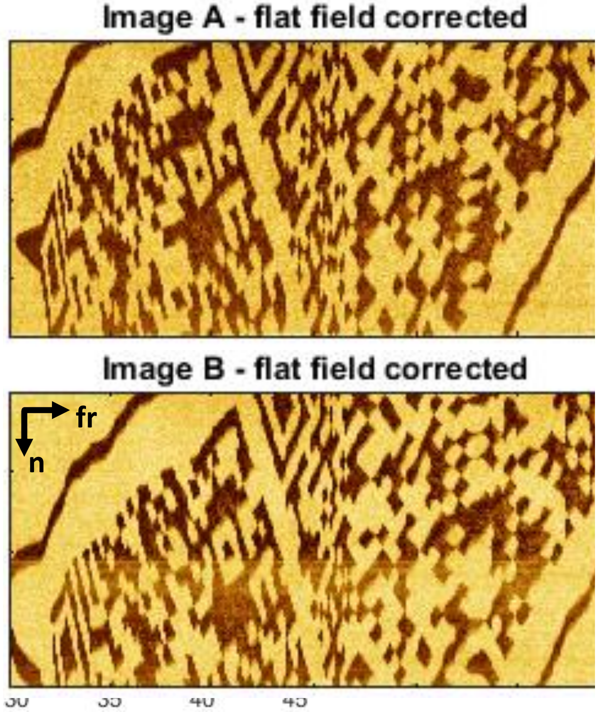

Corrected Images

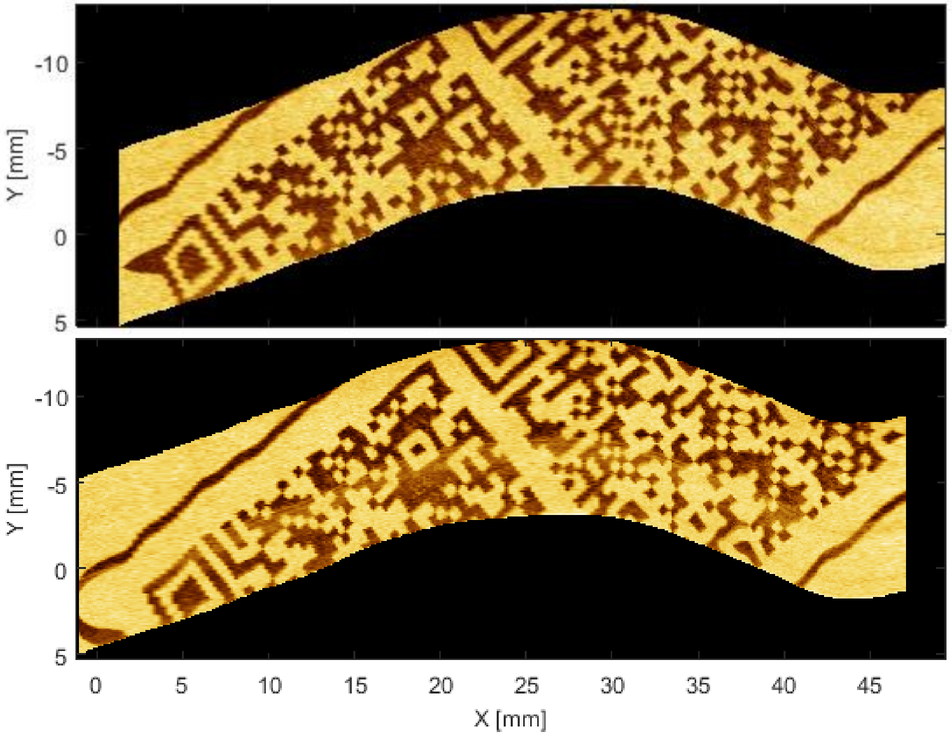

Validation – 1D push at 10 mm/s for kiwi sample

Preprocessed Images

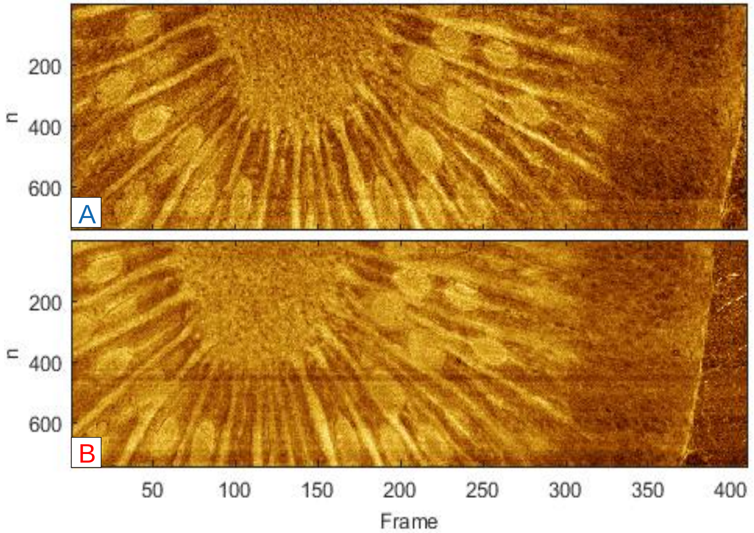

Automated Frame Correlation

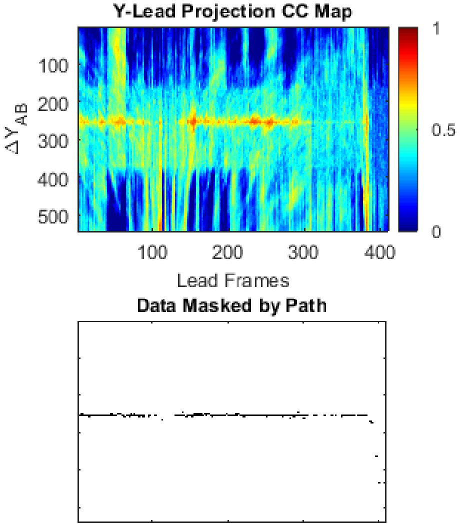

Estimated Velocity & Displacement

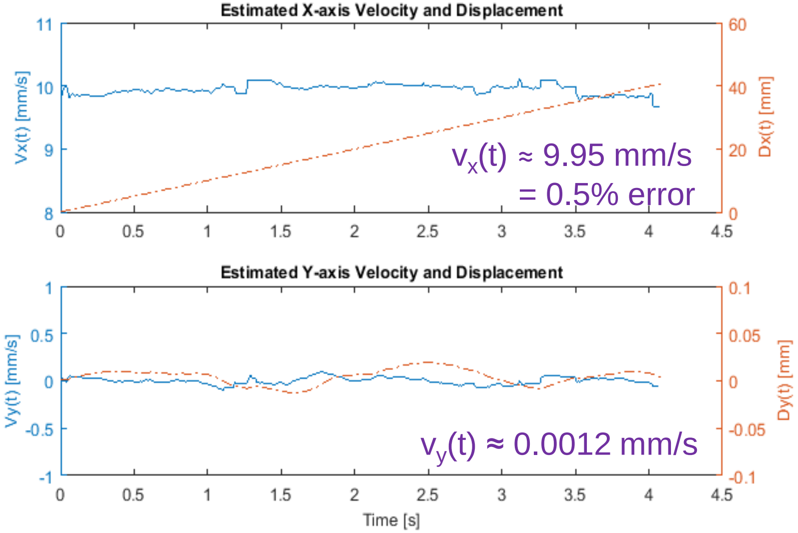

Distortion Corrected Images

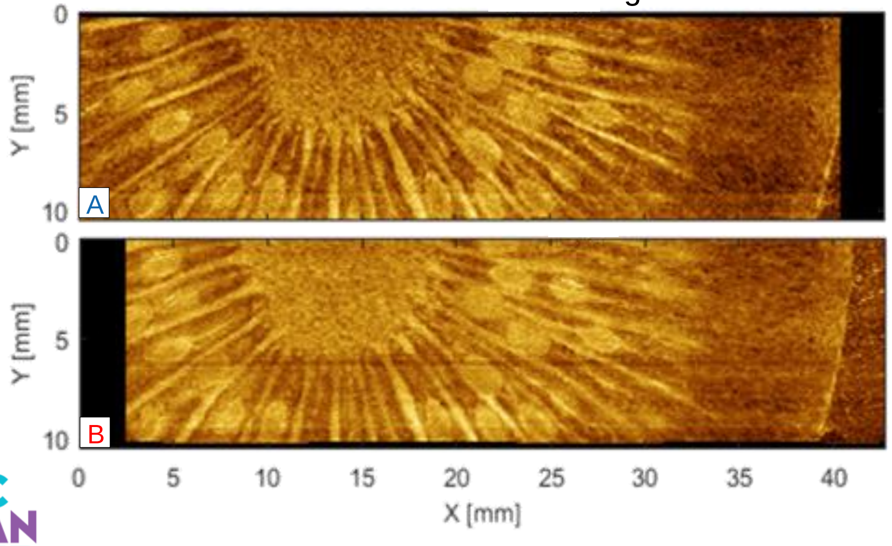

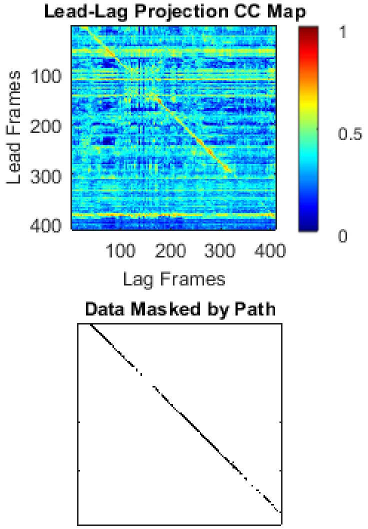

Comparison of Distortion Corrected Images

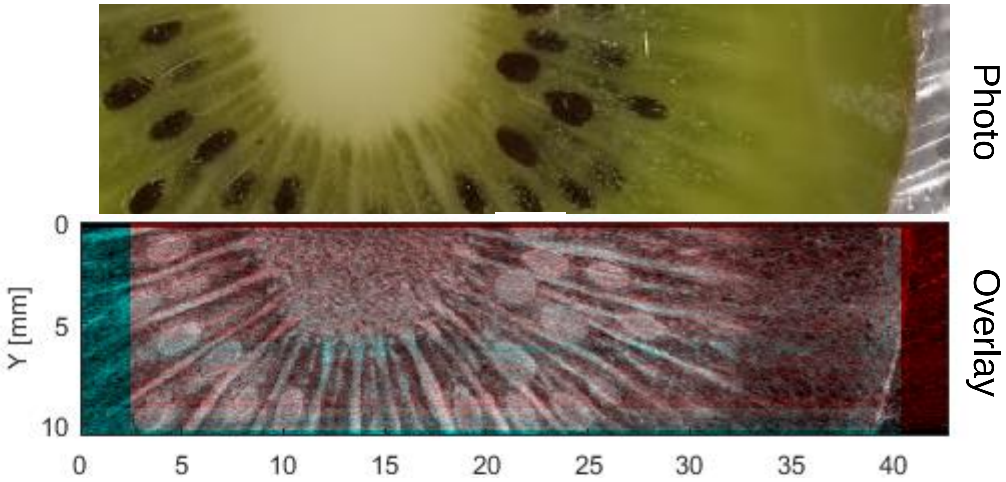

BC CANCER

Validation – 1D push at 10 mm/s for beef tongue sample

Preprocessed Images

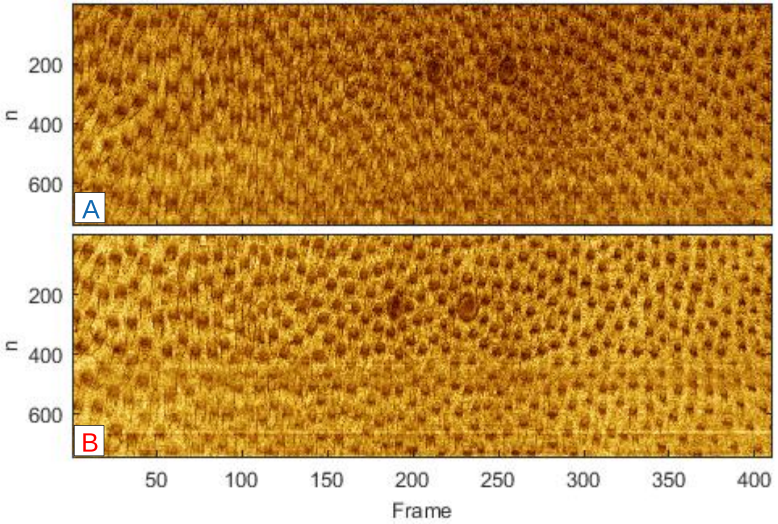

Automated Frame Correlation

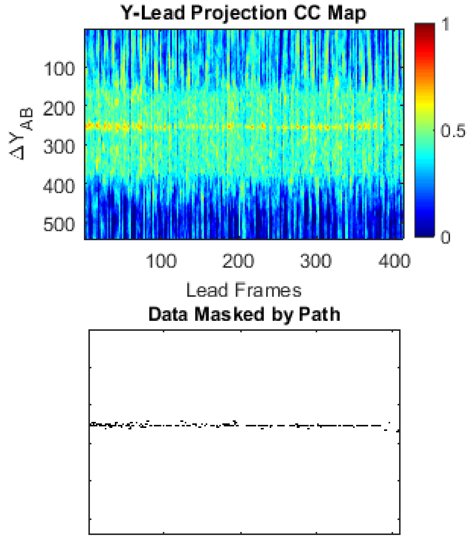

Estimated Velocity & Displacement

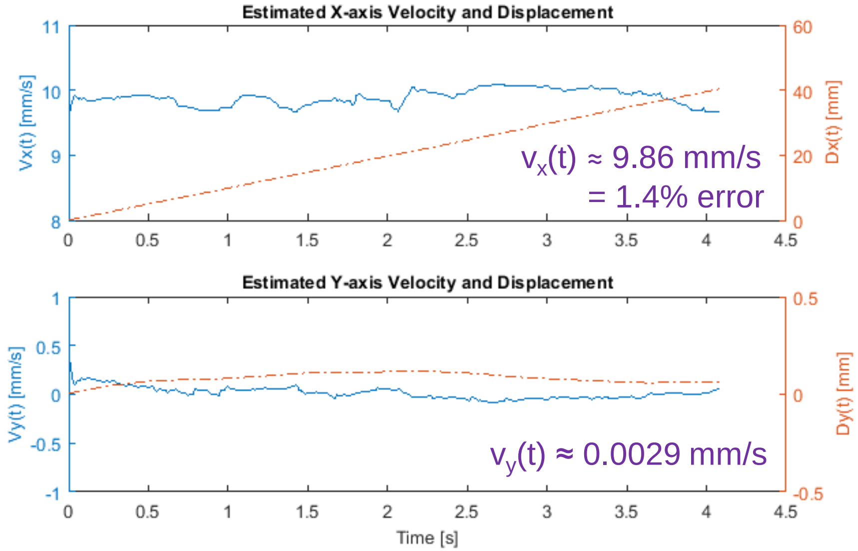

Distortion Corrected Images

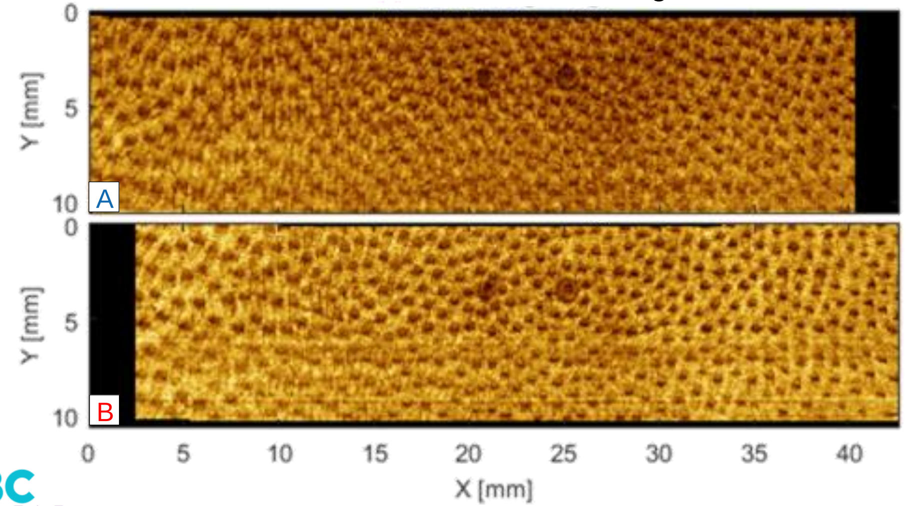

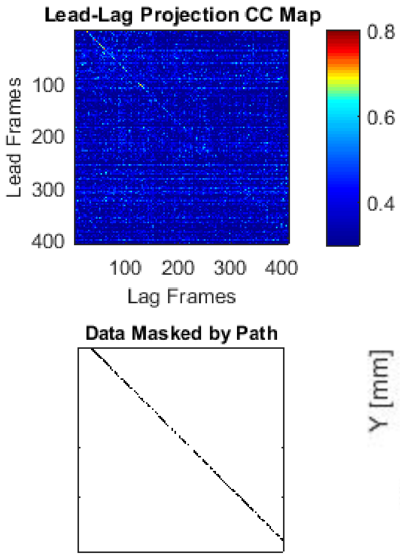

Comparison of Distortion Corrected Images

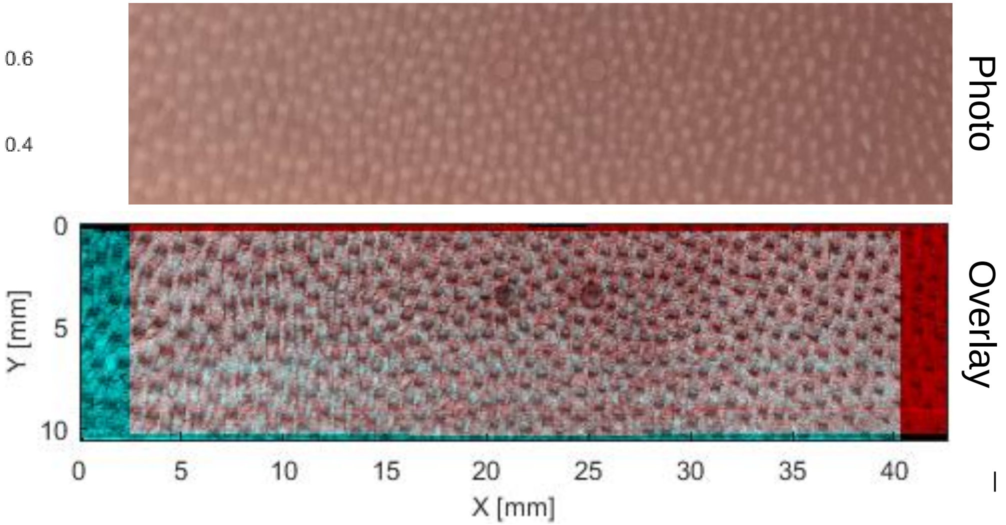

Test– 2D manual actuation scan of a dragon fruit sample

Preprocessed Images

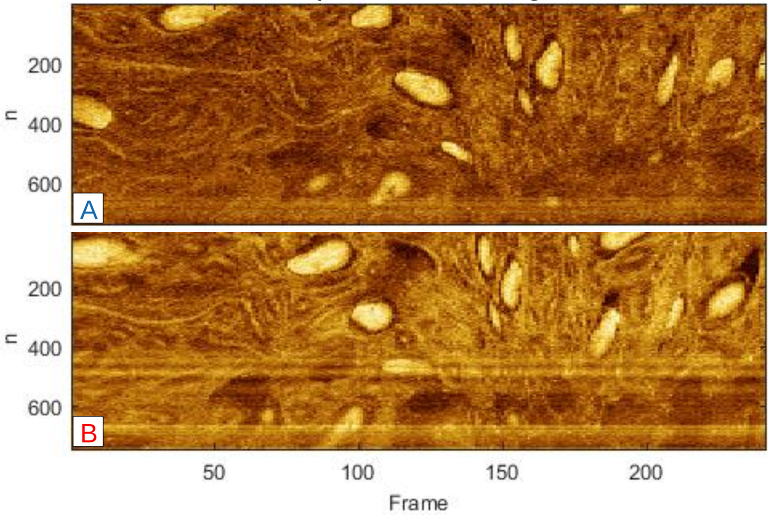

Distortion Corrected Images

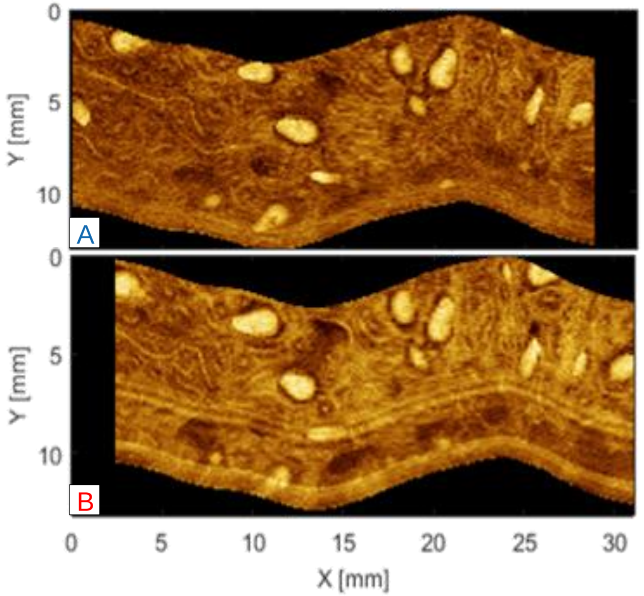

Automated Frame Correlation

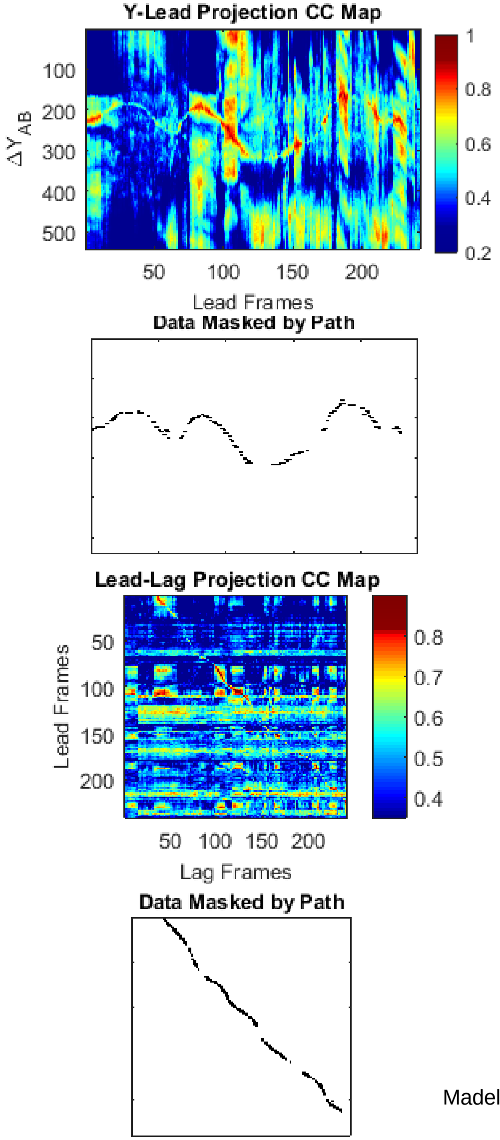

Estimated Velocity & Displacement

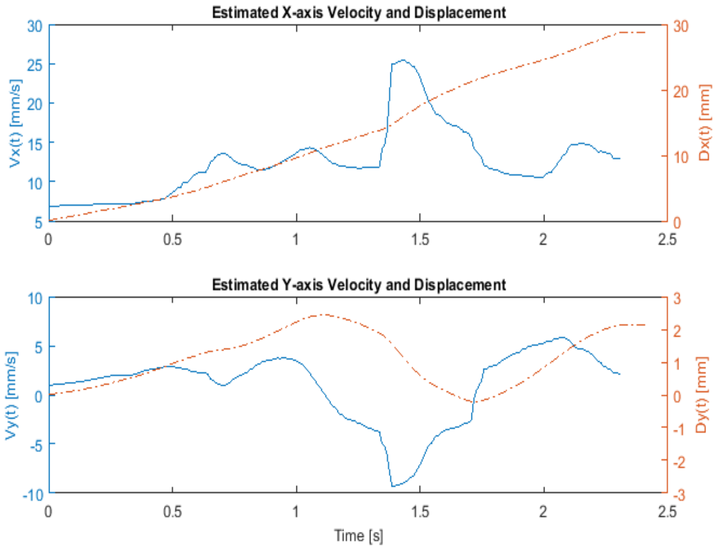

Comparison of Distortion Corrected Images

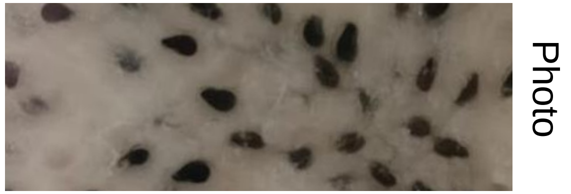

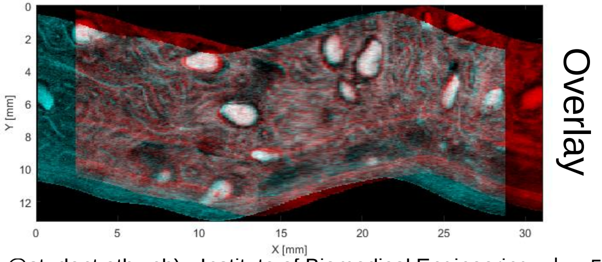

In vivo test – 2D manual actuation scan of a fingerprint

Preprocessed Images

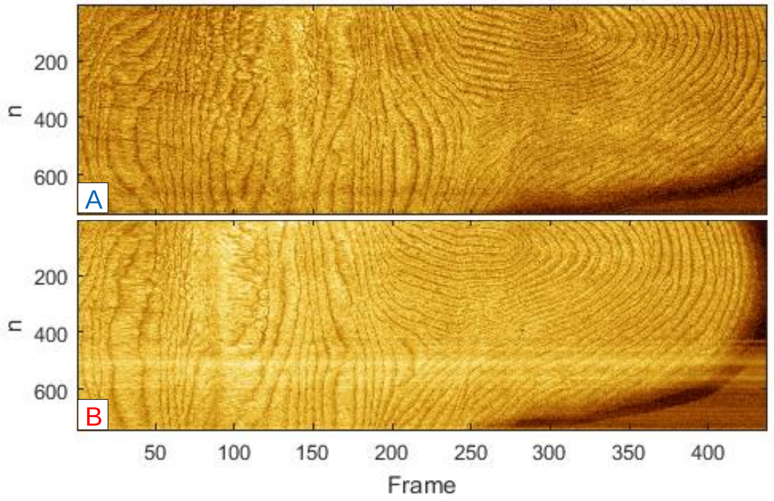

Distortion Corrected Images

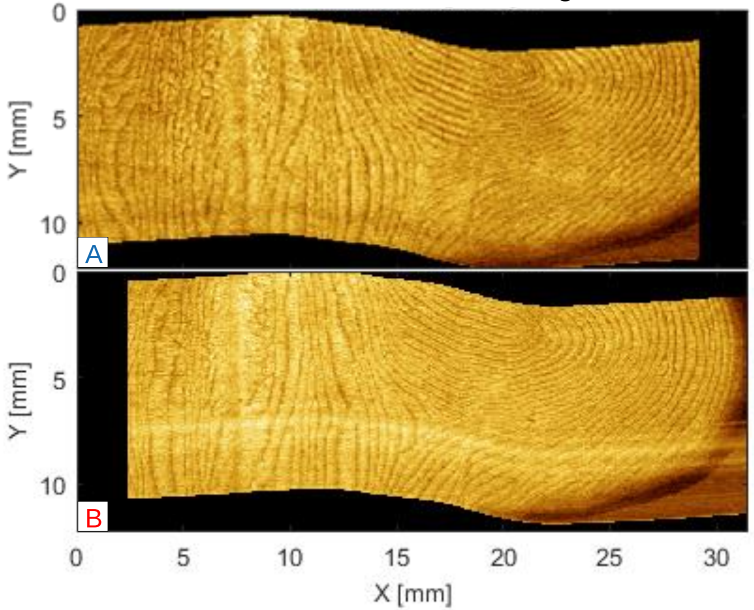

Automated Frame Correlation

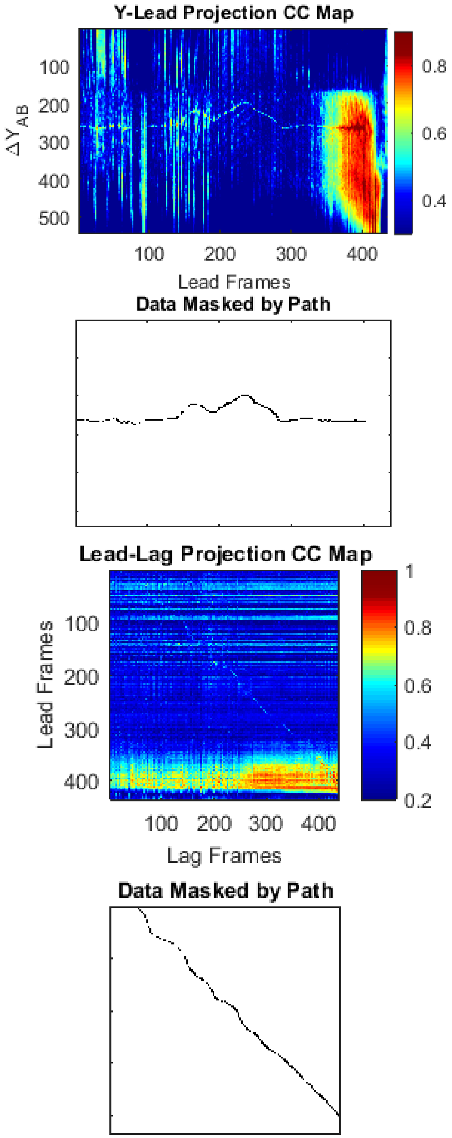

Estimated Velocity & Displacement

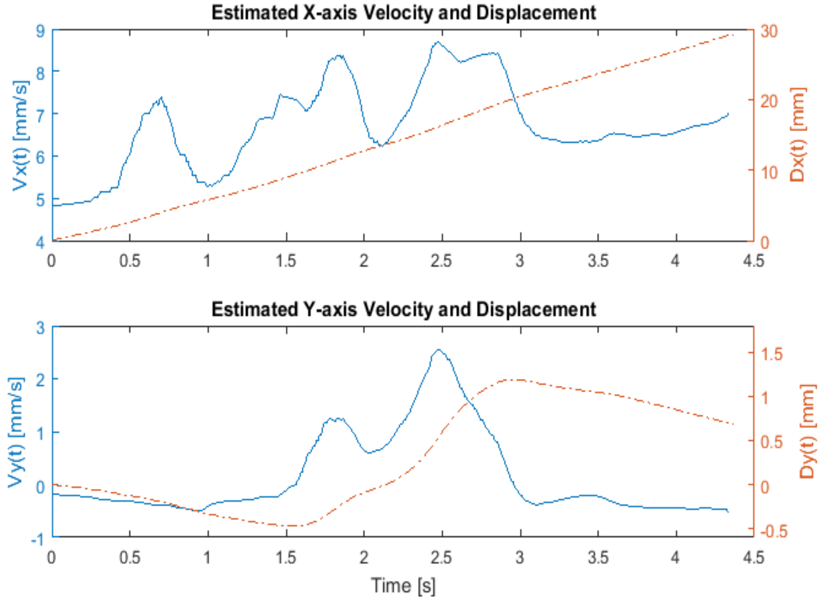

Overlay of Distortion Corrected Images

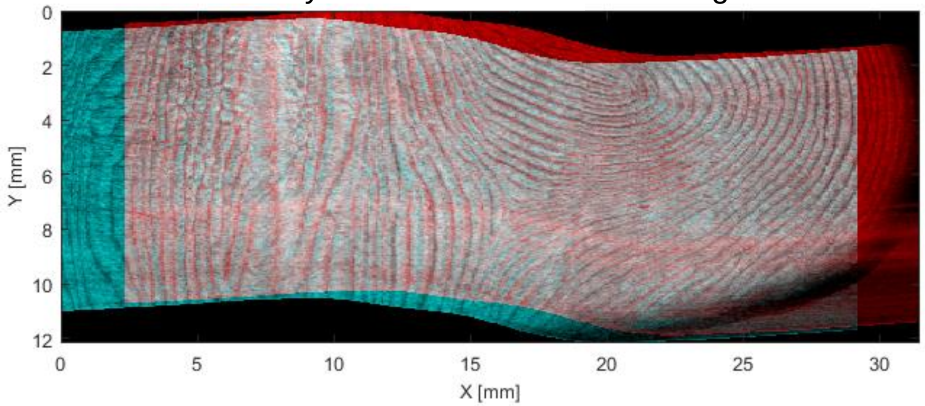

Future Outlook

Advantages

- correct for non-uniform scanning or patient or clinician motion w/o additional sensors
- simplified scan pattern allows for automated correction, approaching real-time
- can be used for alternative imaging sites, such as skin or oral cavity
- can be used for any point scanning modality

Disadvantages

- twice data bandwidth required for imaging
- estimation error due to averaging across large beam separation

Future Work

- improve algorithm for robustness
  - potentially machine learn from this initial guess
  - utilize the retrace region - different waveform
- simulate to find optimal scanning parameters
  - find ideal beam separation to implement
- implement in real-time
- extend to non-monotonic v_x
- extend to 3D
- investigate other implementations for more potential applications

ETH zürich

Thank you, questions?

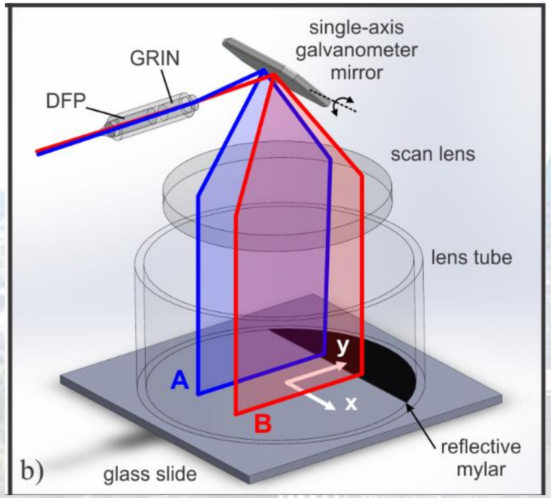

Automated Frame Correlation

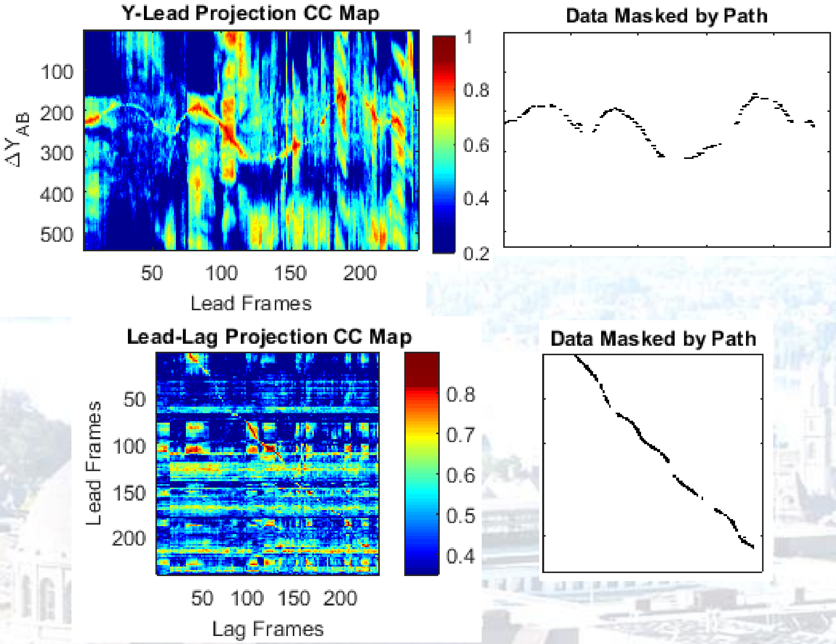

Estimated Velocity & Displacement

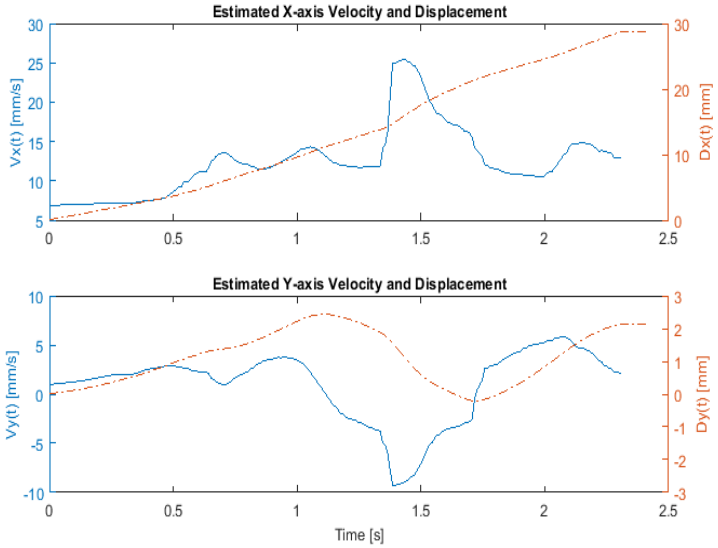

Preprocessed Images

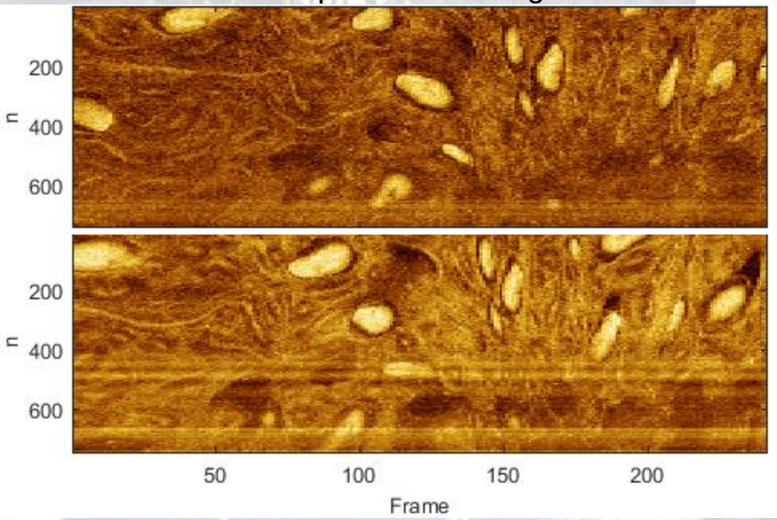

Distortion Corrected Images

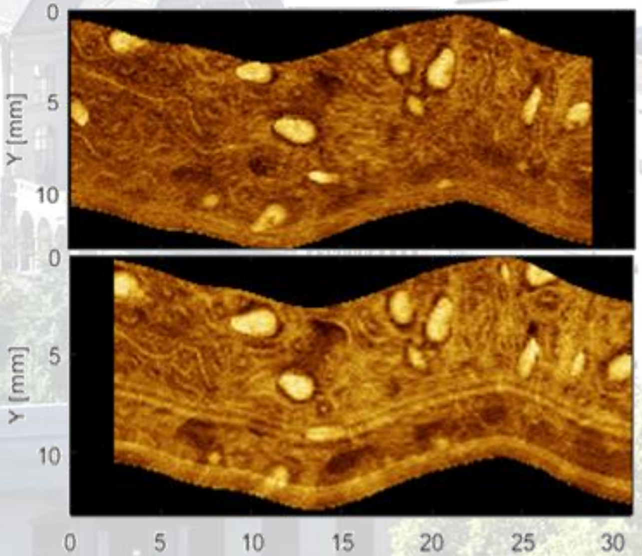

Comparison of Distortion Corrected Images

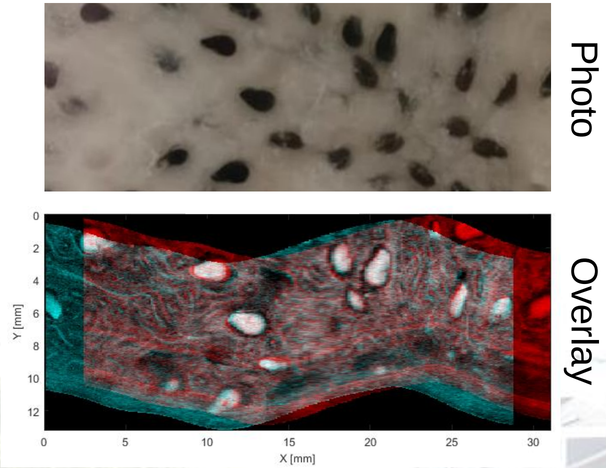

Contact information

ETH Zurich
Institute for Biomedical Engineering
ETZ Gloriastrasse 35
8092 Zürich Switzerland
http://www.biomed.ee.ethz.ch/

Optical Cancer Imaging Lab
BCCRC Department of Integrative Oncology
675 West 10th Ave
Vancouver B.C. V5Z 1L3 Canada
http://www.biophotonics.bccrc.ca/

Madeline Harlow
ETHZ Masters Student
Institute for Biomedical Engineering
mharlow@student.ethz.ch
mharlow@bccrc.ca

Dr. Anthony Lee
Staff Scientist
Optical Cancer Imaging Lab
alee@bccrc.ca

References

[1] http://www.clipartpanda.com/categories/agenda-clip-art-free
[2] S. Optronics. (19.02). *Scan Heads (Marking Heads)*. Available: http://www.sintecoptronics.com.sg/index.php/product/index/id/171.html
[3] A. M. D. Lee, L. Cahill, K. Liu, C. MacAulay, C. Poh, and P. Lane, "Wide-field in vivo oral OCT imaging," *Biomedical Optics Express,* Article vol. 6, no. 7, pp. 2664-2674, Jul 2015.
[4] M. J. Gora *et al.*, "Tethered capsule endomicroscopy enables less invasive imaging of gastrointestinal tract microstructure," *Nature Medicine,* Article vol. 19, no. 2, pp. 238-240, Feb 2013.
[5] B. Lau, R. A. McLaughlin, A. Curatolo, R. W. Kirk, D. K. Gerstmann, and D. D. Sampson, "Imaging true 3D endoscopic anatomy by incorporating magnetic tracking with optical coherence tomography: proof-of-principle for airways," *Optics Express,* Article vol. 18, no. 26, pp. 27173-27180, Dec 2010.
[6] X. Liu, Y. Huang, and J. U. Kang, "Distortion-free freehand-scanning OCT implemented with real-time scanning speed variance correction," *Optics Express,* Article vol. 20, no. 15, pp. 16567-16583, Jul 2012.
[7] A. Lee, G. Hohert, P.T. Angkiriwang, C. MacAulay, P. Lane. "Dual-beam manually-actuated distortion-corrected imaging (DMDI) with micromotor catheters". Optics Express 22164, Vol. 25, No. 18, 4 Sep 2017.
[8] W. Drexler, J.G. Fujimoto. "Optical Coherence Tomography Technology and Applications". Second Edition. Springer International Publishing, Switzerland, 2015.

Appendix I

Simulations

Constructing Simulated Distorted Images

- Construct an effective beam path
  - Parameterized scanning pattern
  - Simulated velocity profiles
- Trace simulated path onto sample image
  - Here a tiled QR code
- Add noise
  - Gaussian blurring for PSF (σ=0.5)
  - Speckle noise for OCT imaging (var_A = 0.01 var_B = 0.02)

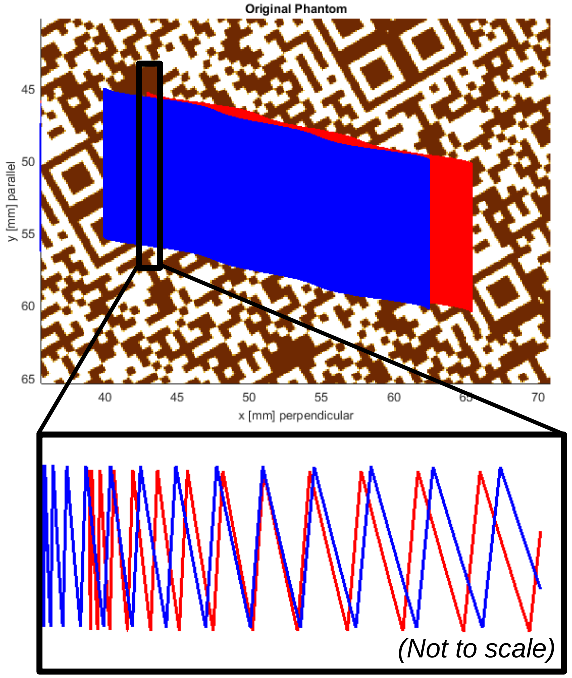

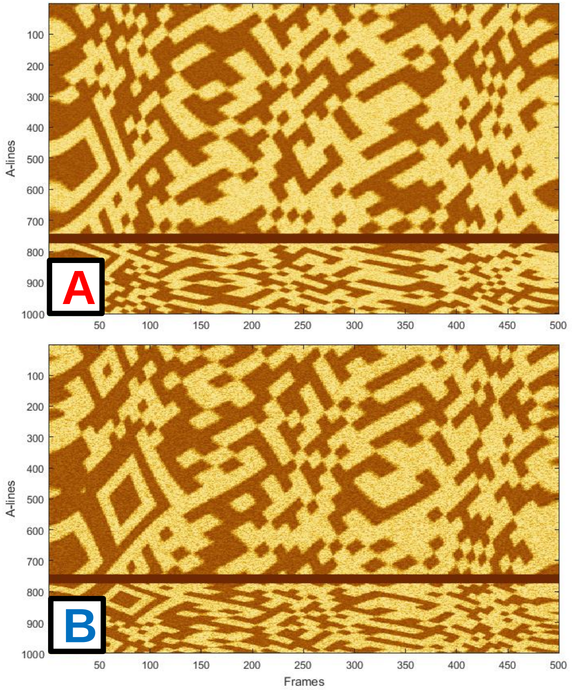

- Error metrics for comparison:
  - RMSE – direct error comparison
  - Confidence – indirect error assessment

$$RMSE = \sqrt{\frac{1}{N_v}\sum_{i=1}^{N_v}\left(v_{est,i} - v_{sim,i}\right)^2}, \qquad N_v, i \in \mathbb{Z}$$

$$Confidence = \frac{\sum_{j=1}^{N_{pairs}} CC_j}{N_{frames}}, \qquad j \in \mathbb{Z}$$

BC CANCER

Simulation 1: Velocity limits for 3 beam separations

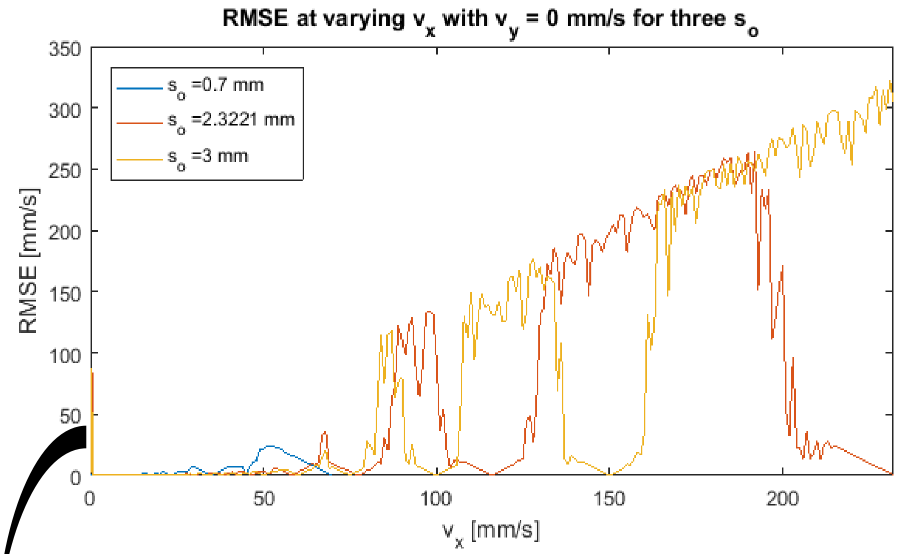

RMSE is plotted for three beam separations for a range of constant v_x, up until the $v_{x,max}$ corresponding to that beam separation.

These results indicate there is an effective ideal range of v_x depending on beam separation to achieve high correction accuracy.

Additionally, ideal accuracy is achieved at integer divisions of $v_{x,max}$ corresponding to that beam separation.

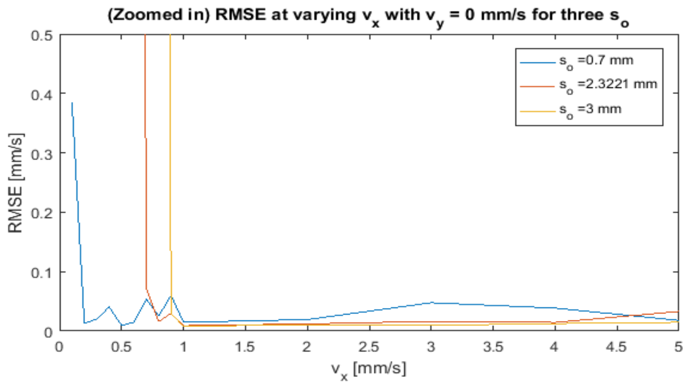

Zoomed in plot of above to observe the effects of beam separation on correction accuracy. Smaller beam separations are sensitive to smaller v_x but less sensitive to higher v_x compared to larger beam separations.

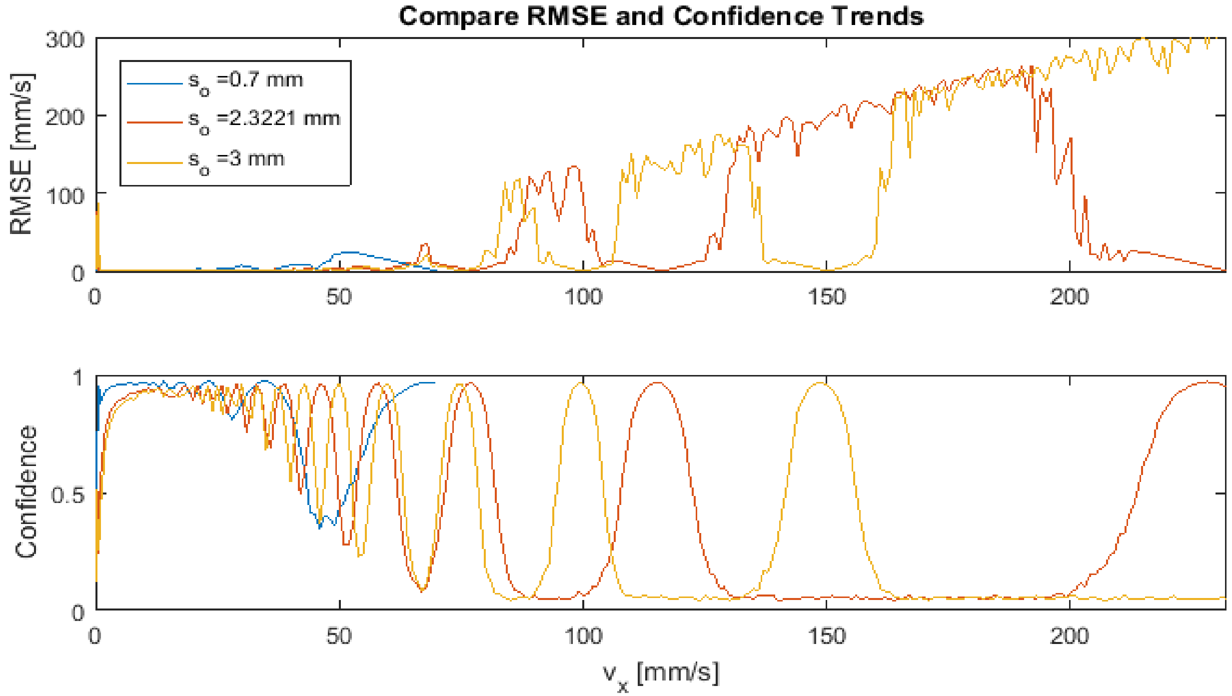

Confidence [bottom] inversely follows the same trends as RMSE [top], suggesting confidence may be used as a measure of performance when ground truth is not available.

Simulation 2: Effects of v_x, v_y, and beam separation

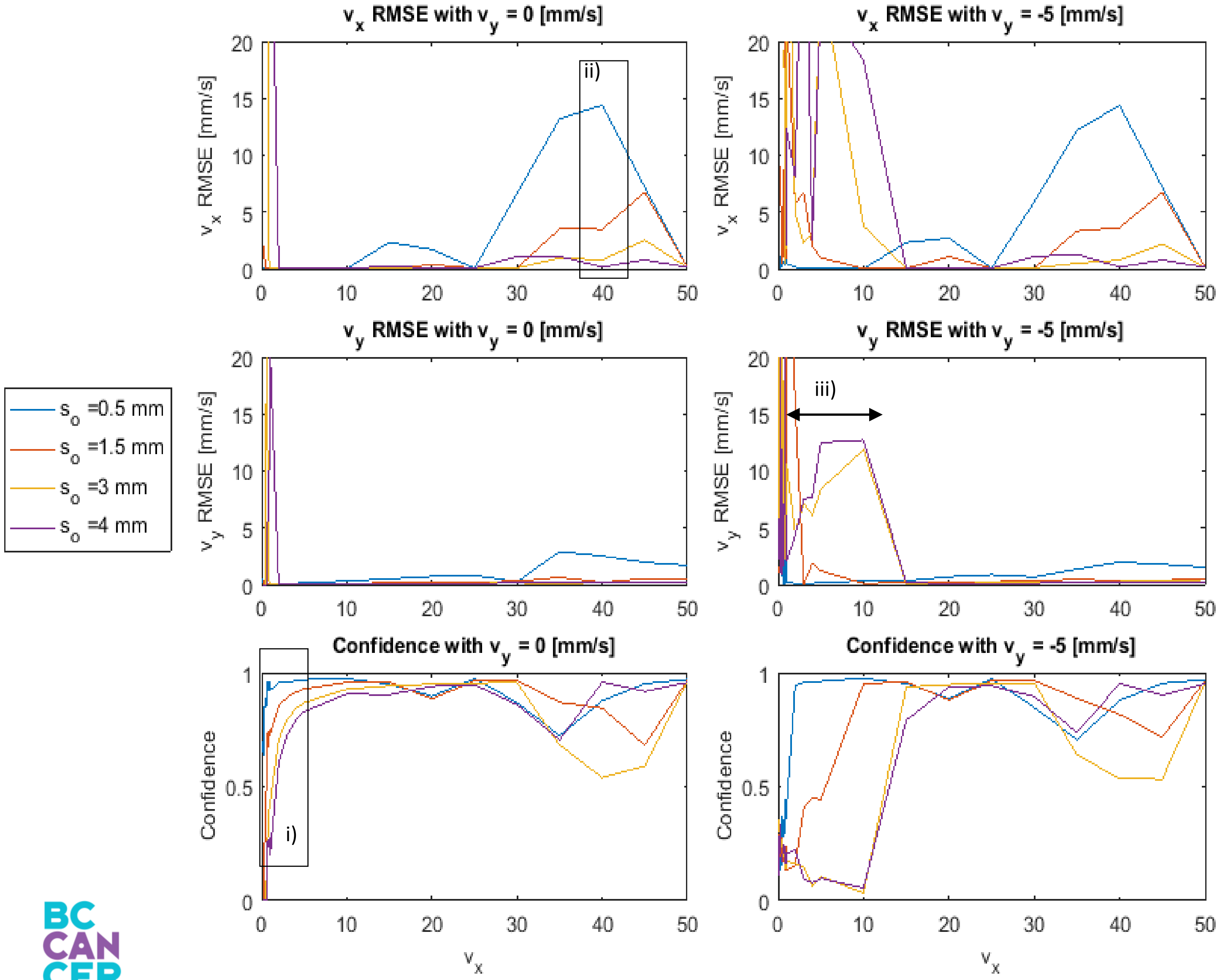

Compare correction results for two cases: v_y = 0mm/s [left] and v_y = -5 mm/s [right]. RMSE is calculated and plotted for both v_x estimates [top] and v_y estimates [middle] for each simulation as well as the confidence [bottom].

i) Small beam separations are more accurate at very small v_x while ii) large beam separations are more accurate at high v_x.

iii) Increasing v_y appears to increase the minimum detectable v_x.

Simulation 3: Effects of varying v_x and beam separation

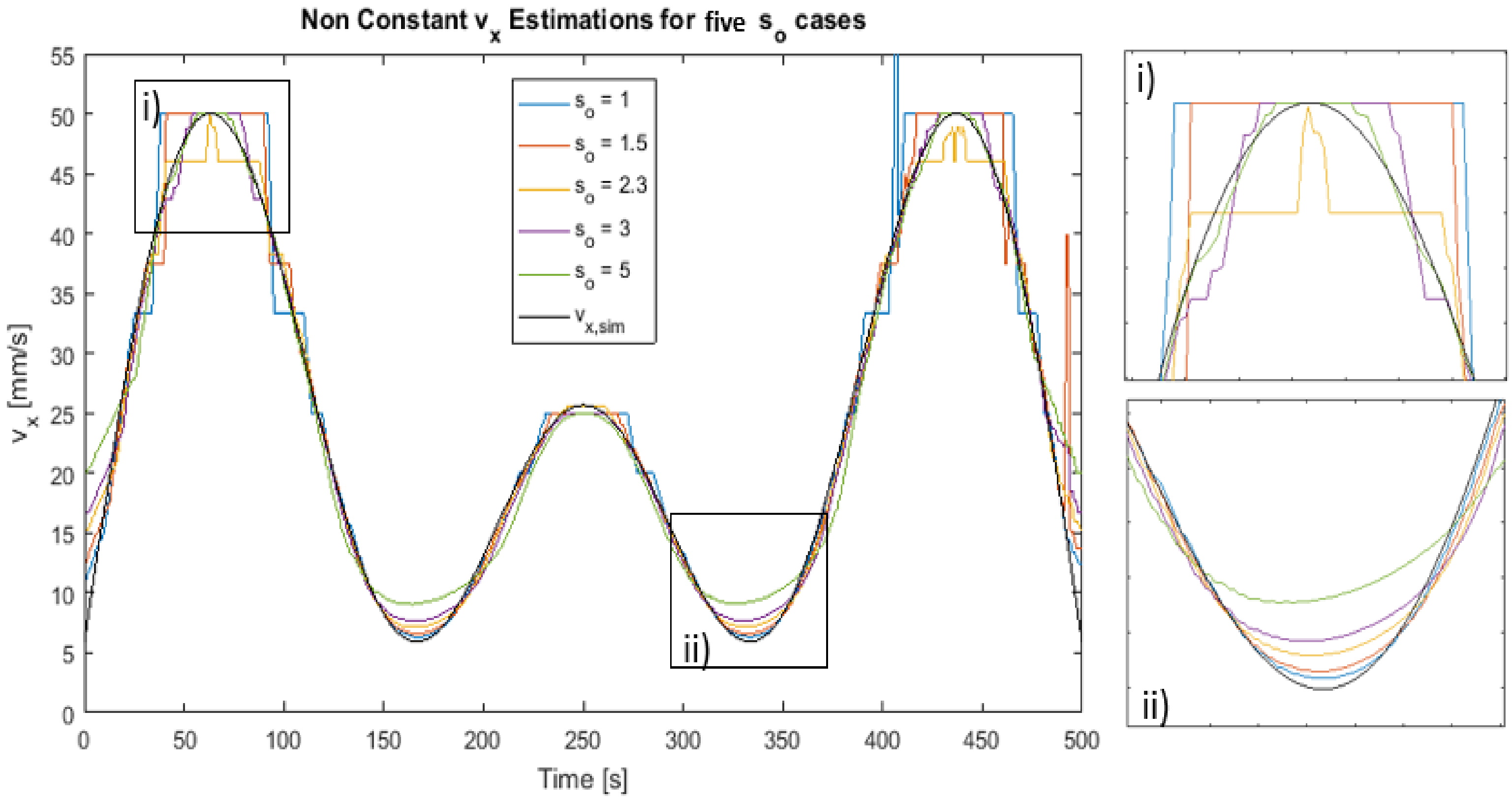

Estimated variable v_x profile with different beam separations. The simulated v_x profile is a modified sinusoidal function plotted in black and the estimated velocity profile corresponding to different beam separations are plotted in colour.

i) Large beam separations appear to perform better at estimating high v_x peaks.

ii) Smaller beam separations appear to perform better at estimating low v_x peaks.

Simulation 4: Functionality of confidence for biological sample

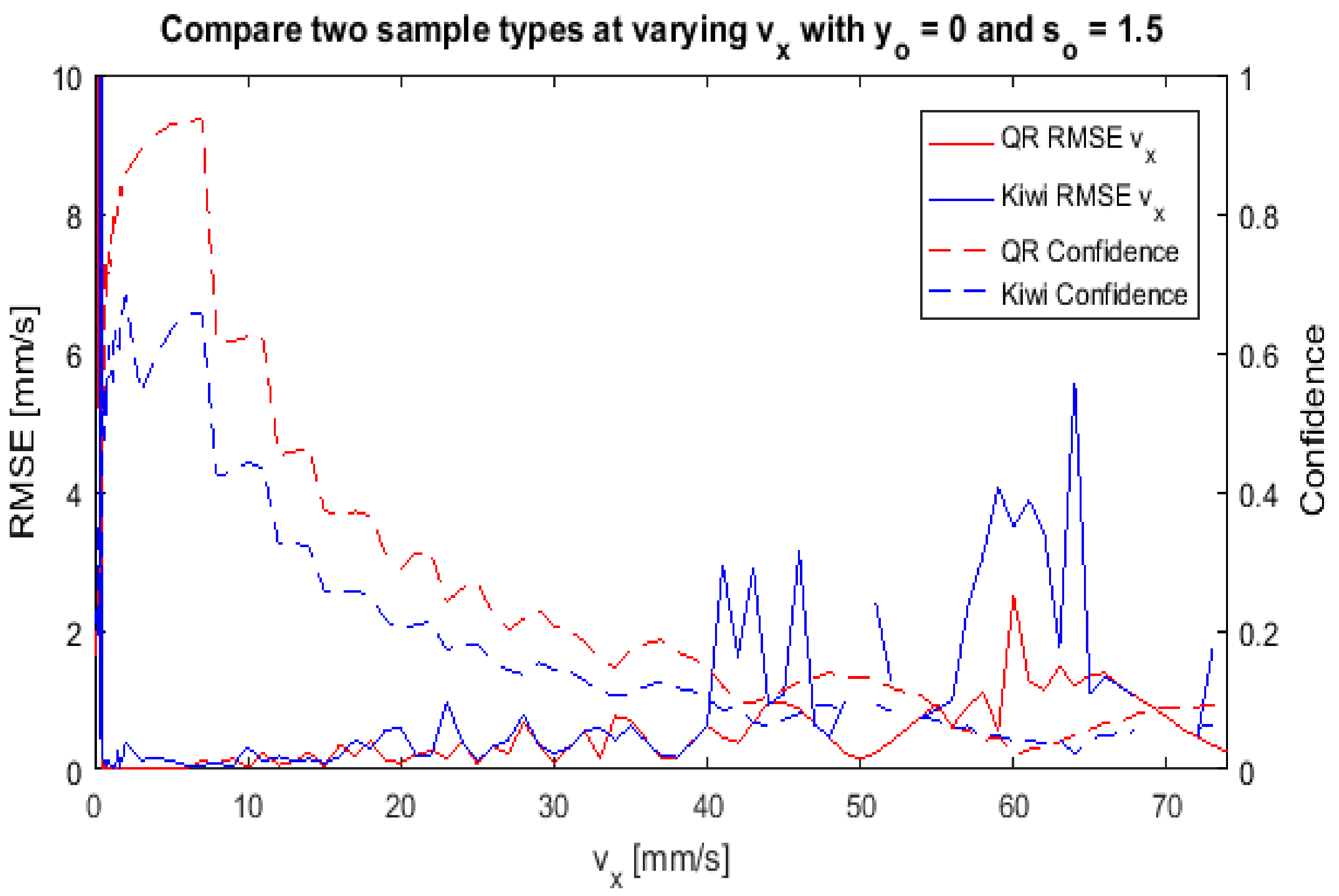

Comparing correction metrics for QR and biological sample. Confidence inversely follows the same trends as RMSE. Further, confidence appears to follow the same trends for both the digitally constructed QR sample and the real images of the biological sample, i.e. kiwi, however at a lower offset

Summary of Simulation Results

Appendix II

DBMC Implementation

Dual Beam Micromotor Catheter - Construction

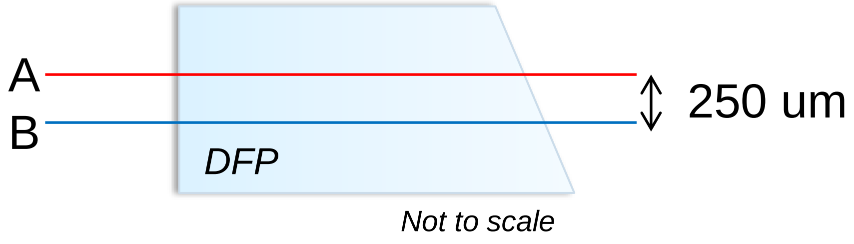

- Dual SMF-28 fiber pigtail (DFP) is aligned to a graded index (GRIN) lens using glass ferrule: both are polished at 8° and anti-reflection coated for 1310 nm
- Two fibers within DFP are separated by 250 um and DFP is separated from GRIN to provide a 3.5 mm distance to target with a 14 um spot
- Target is aluminum coated, 1 mm right angle prism mounted to shaft of 4 mm OD micromotor at approximately 8°.

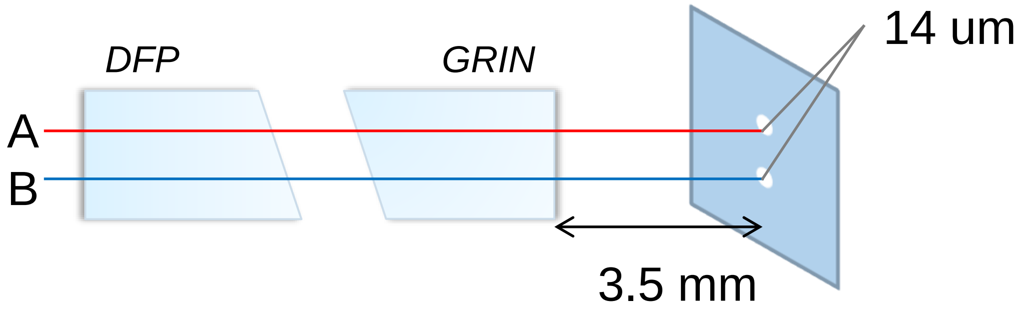

A. Lee (2017)

Dual Beam Micromotor Catheter - Function

- Two beams (A and B) scan mechanically along one dimension [radial, fast axis] with known separation in second dimension [axial, slow axis]
- Catheter is manually pushed or pulled in axial axis
- A and B pass same features at different times providing **scan speed** and **direction**
- Scan speed and direction allows for image remapping and distortion correction

1310nm OCT specific implementation:

MM = 4mm OD micromotor (Namiki)
FPC = flexible printed cable
DFP = double SMF-28 pigtail (8° polish)
GRIN = graded index lens (8° polish)

overall catheter diameter = 4.7mm

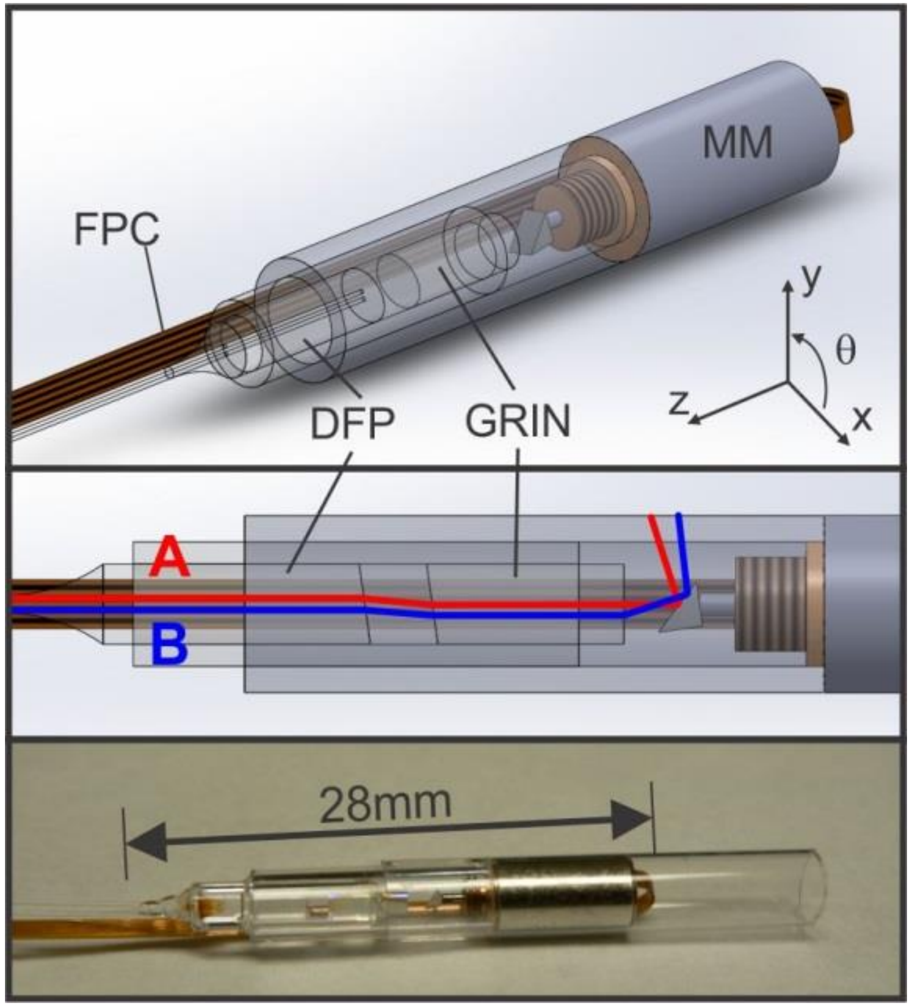

A. Lee (2017)

DBMC Image Acquisition

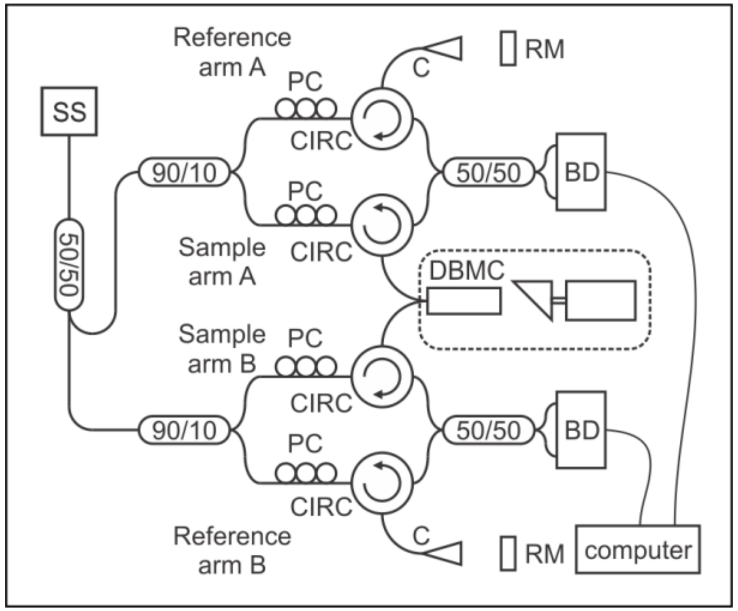

100kHz Axsun source
100Hz MM spin rate
2-channel Alazartech digitizer

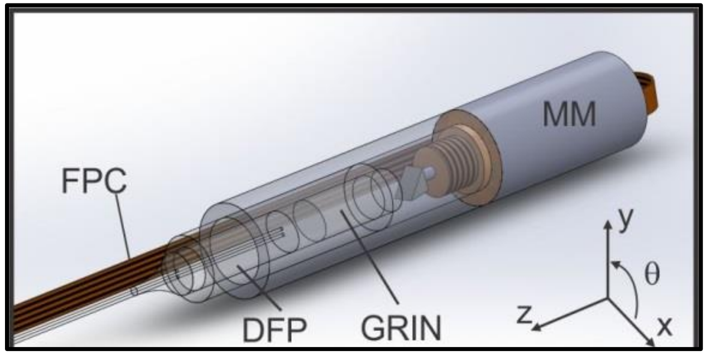

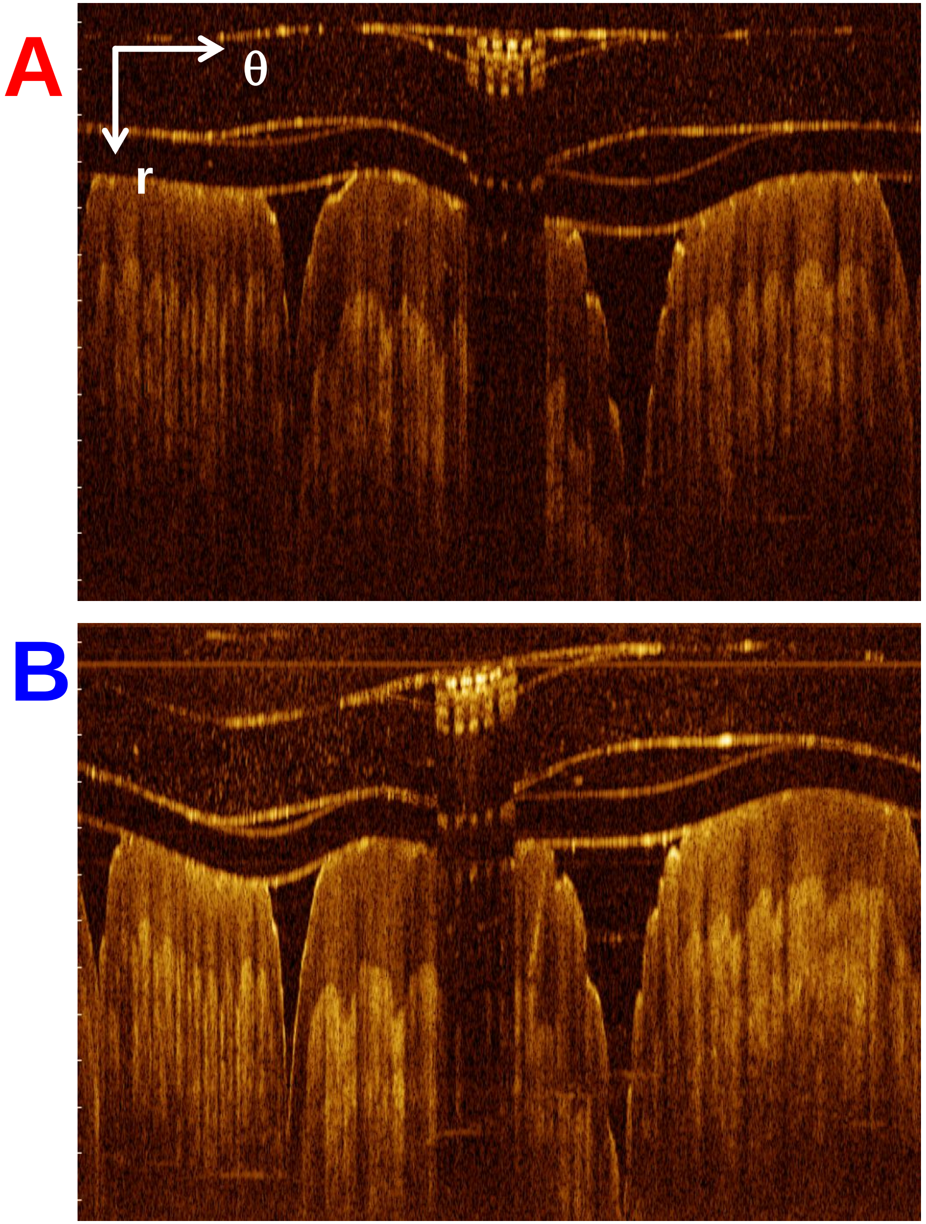

A. Lee (2017)

DBMC - Calibration

phantom

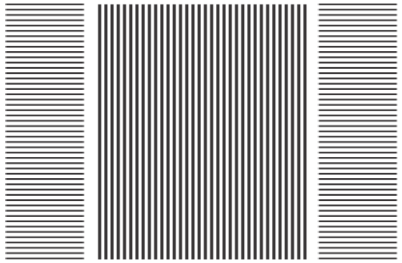

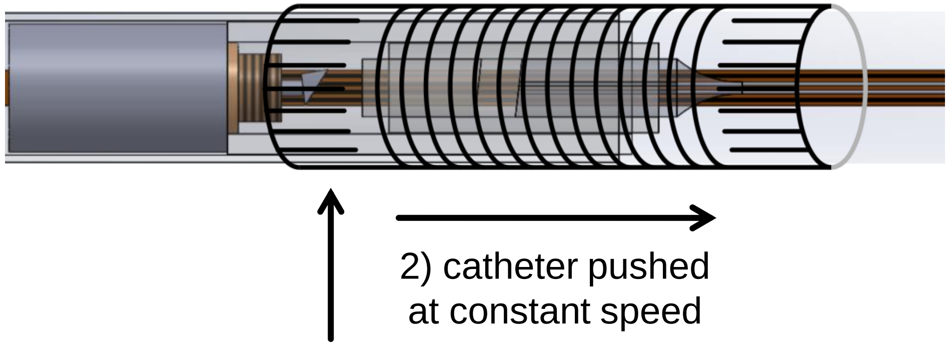

raw *en face*
OCT images

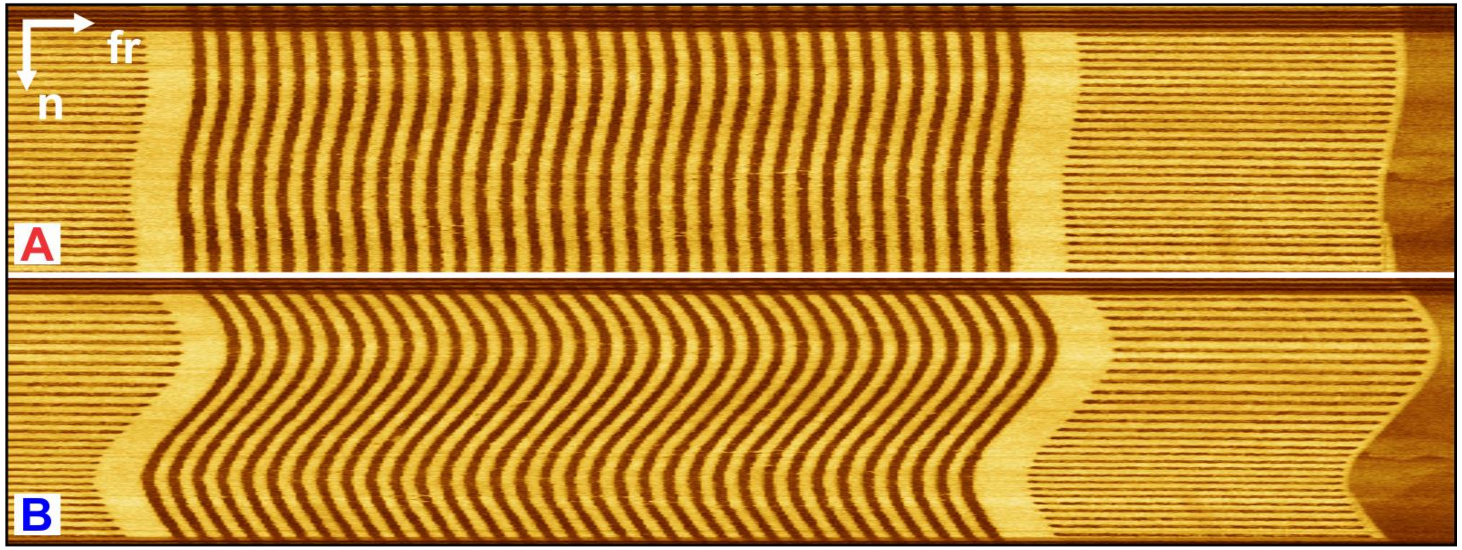

A. Lee (2017)

N → Θ Calibration (DBMC)

(time)

phantom

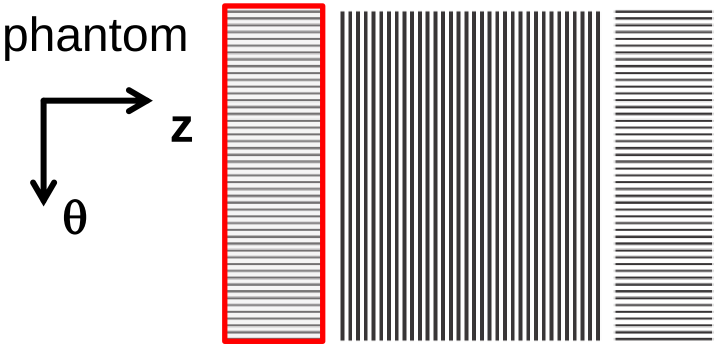

catheter
stationary here

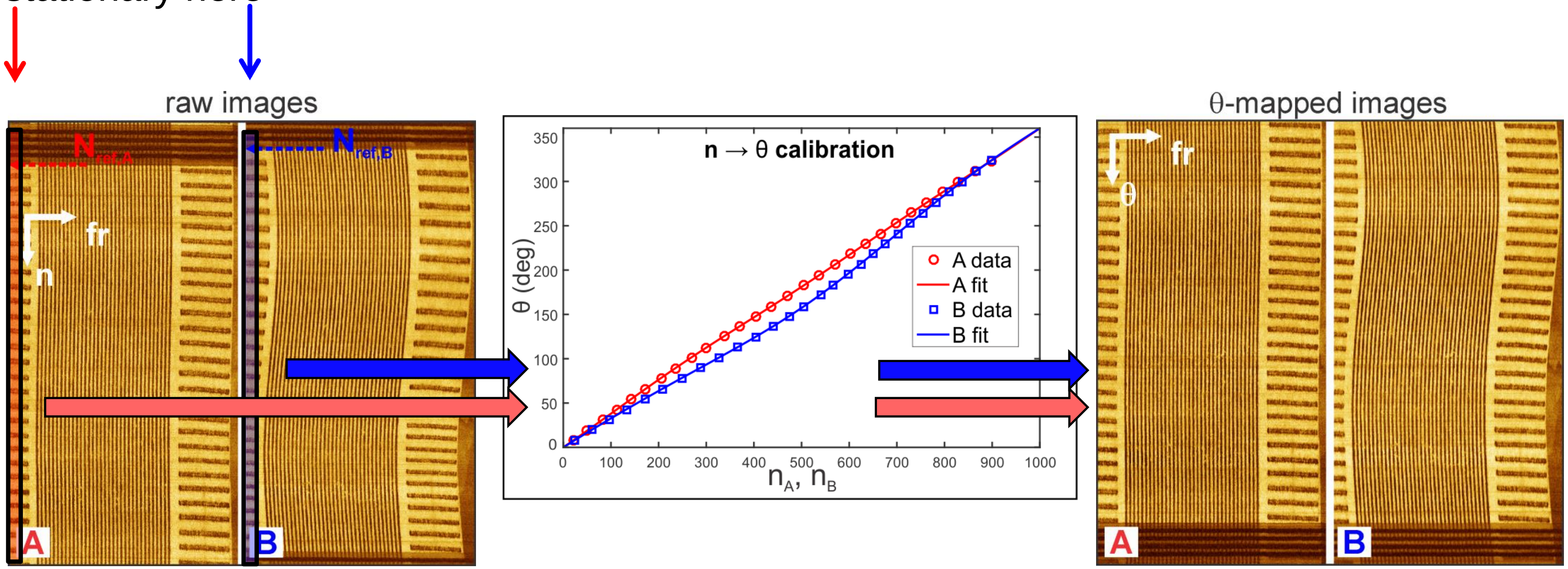

A. Lee (2017)

Beam Path Calibration (DBMC)

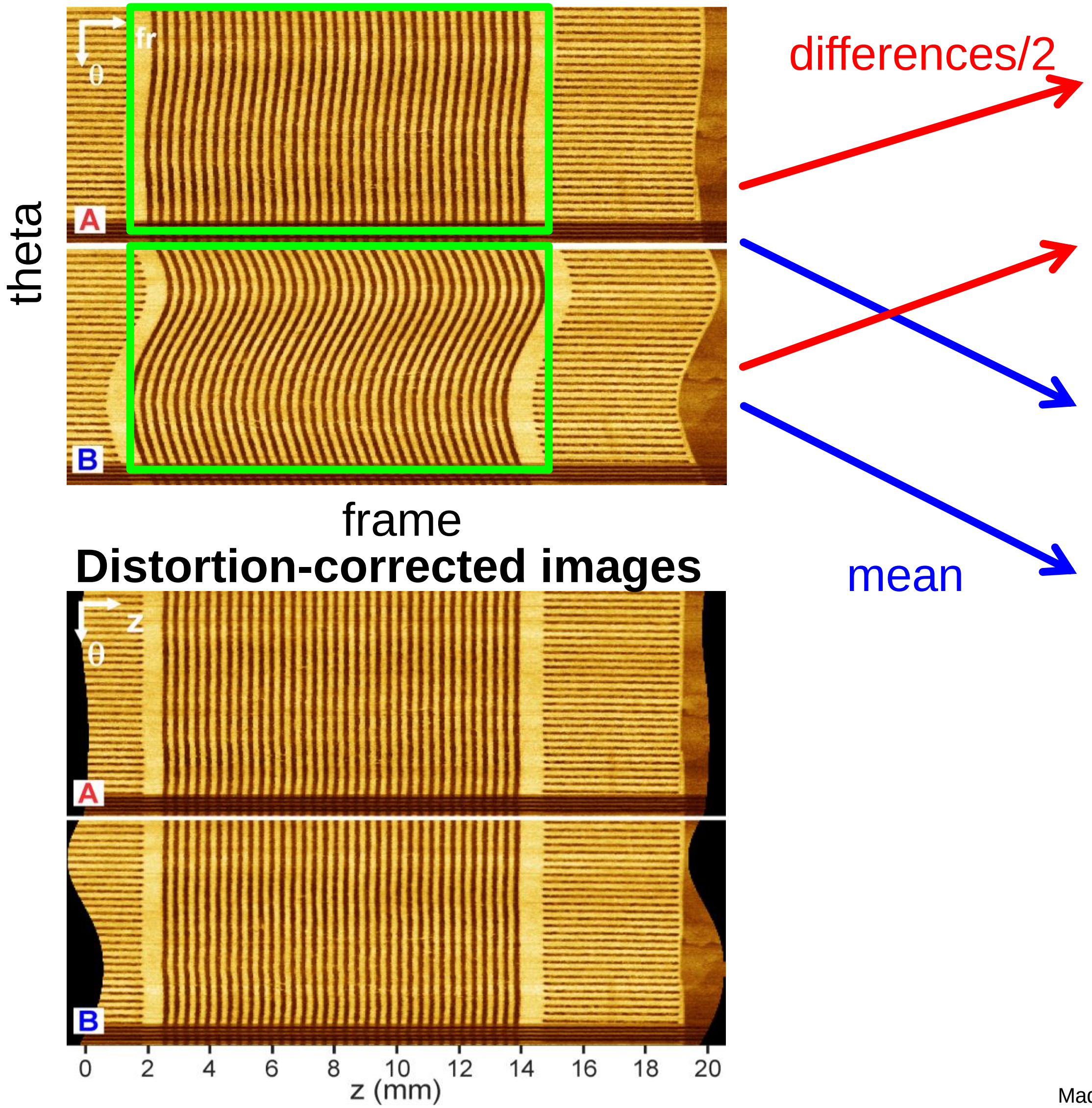

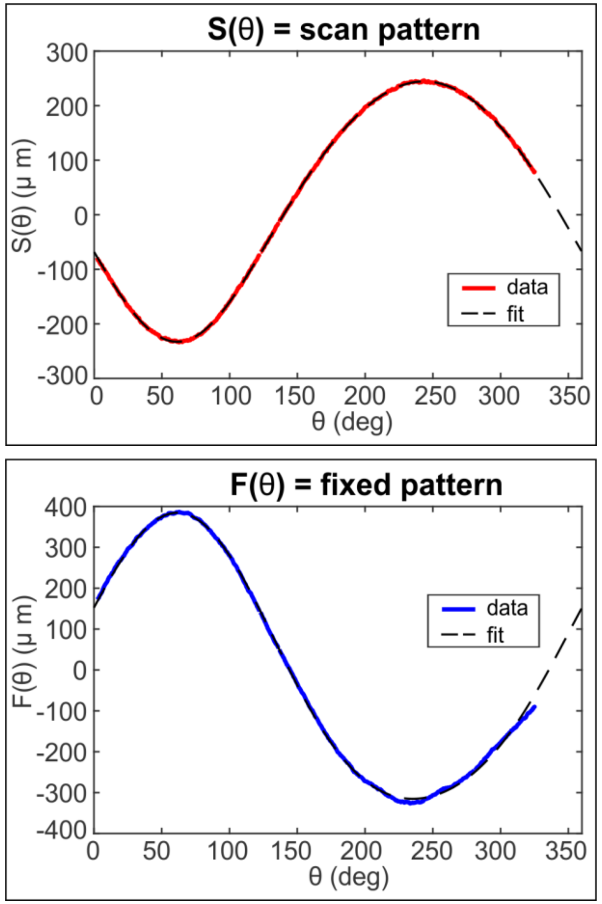

$$z_A(\theta,t) = z_{DBMC}(t) - S(\theta) - F(\theta)$$

$$z_B(\theta,t) = z_{DBMC}(t) + S(\theta) - F(\theta)$$

$$z_{DBMC}(t) = \int v_z(t')\,dt'$$

A. Lee (2017)

BC CANCER

Distortion Correction Validation (DBMC)

phantom: 1mm checkerboard original images:

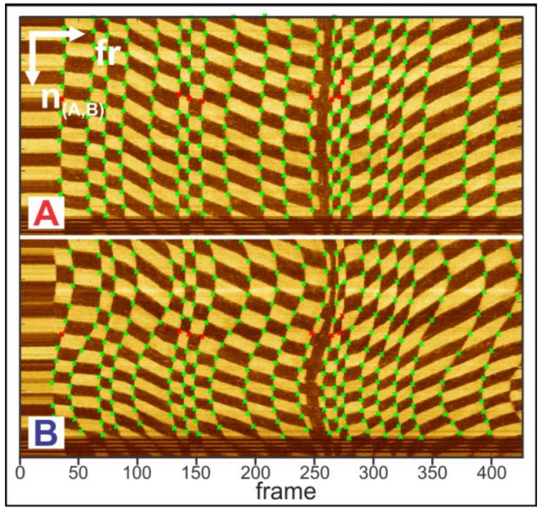

manual control point registration:

$$[(n_A,\ fr_A),\ \ (n_B,\ fr_B)]_j$$

$$[(\theta_A, t_A), (\theta_B, t_B)]_j$$

$$\overline{\omega}_{AB,j} = \frac{\theta_{second,j} - \theta_{first,j}}{\left| t_{A,j} - t_{B,j} \right|}$$

$$\overline{\upsilon}_{z,AB,j} = \frac{S\left(\theta_{A,j}\right) + S\left(\theta_{B,j}\right)}{\left| t_{A,j} - t_{B,j} \right|}$$

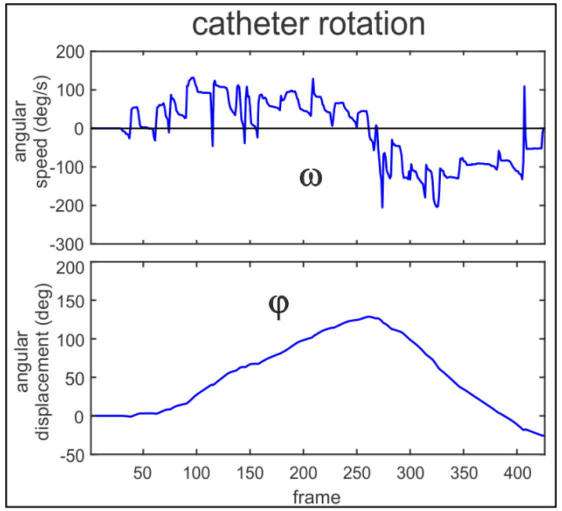

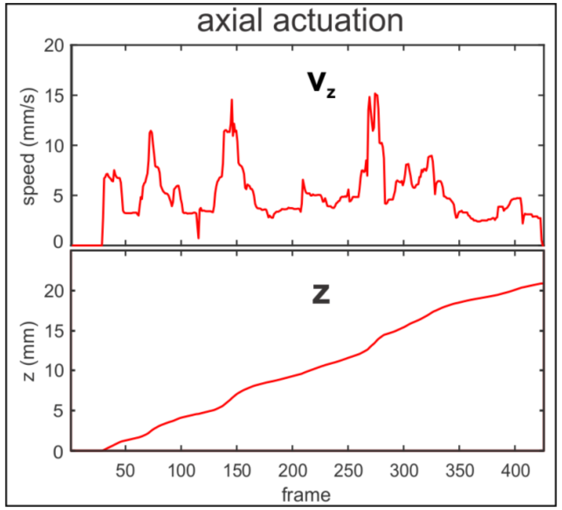

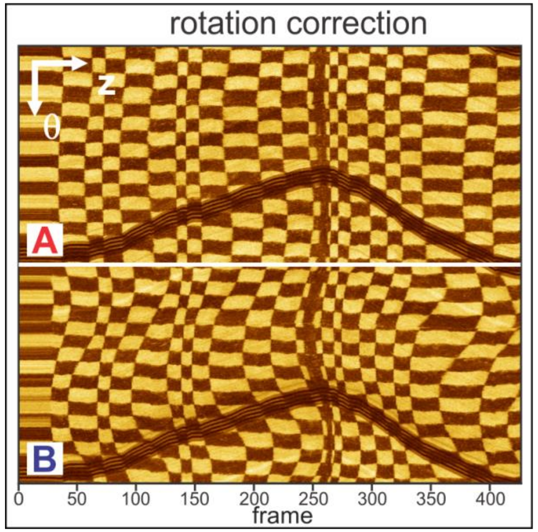

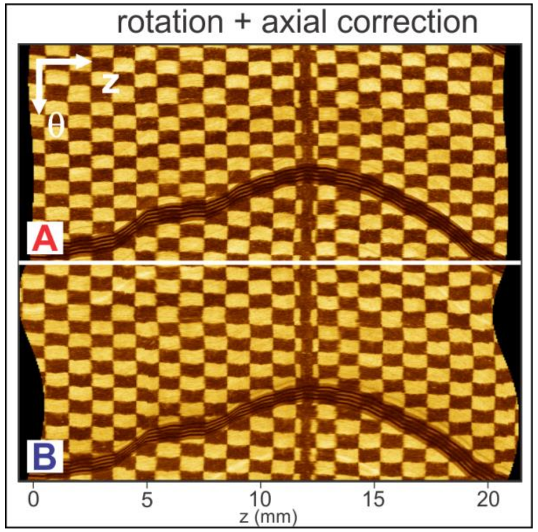

A. Lee (2017)

BC CANCER

Finger Imaging (DBMC)

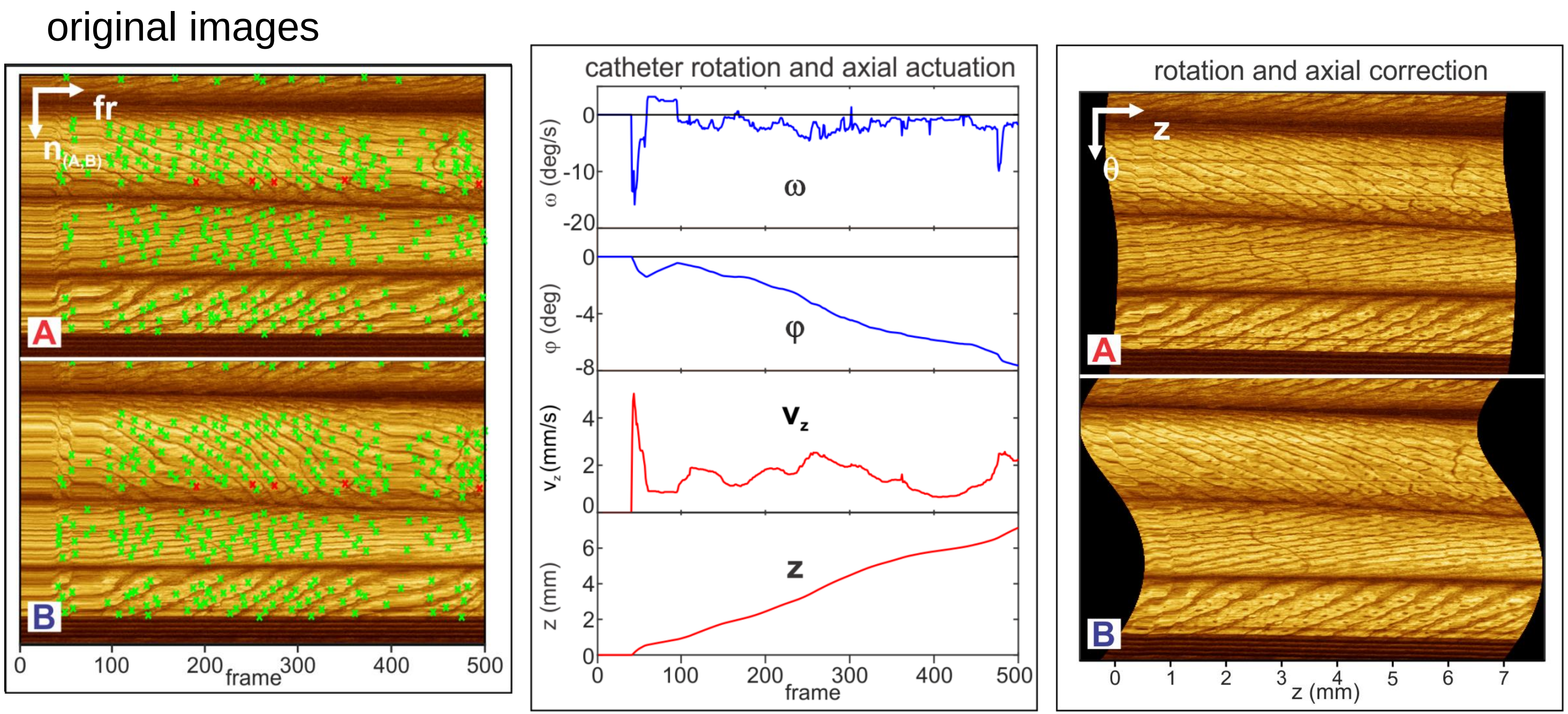

A. Lee (2017)

Multiplexed DBMC

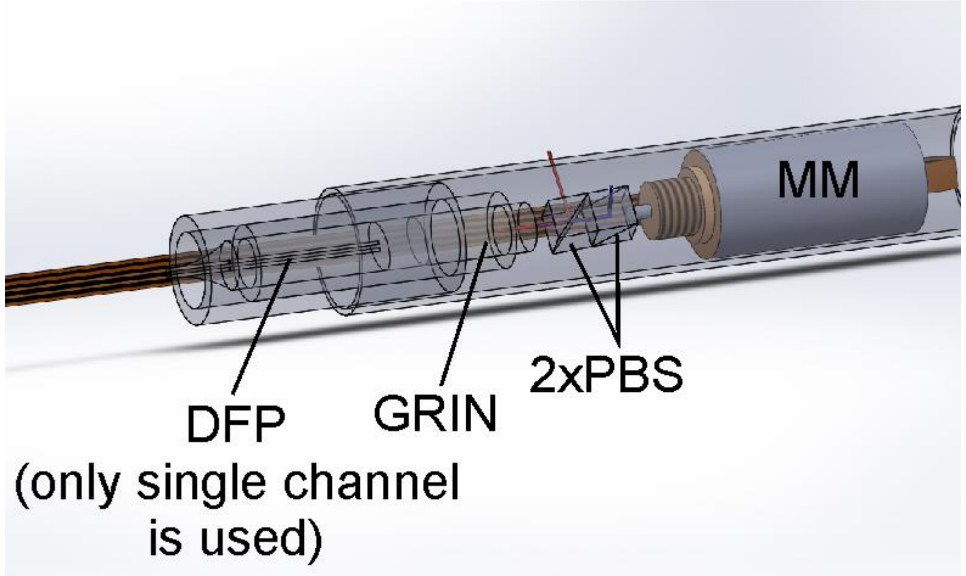

PBS's are oriented 90 degrees relative to each other

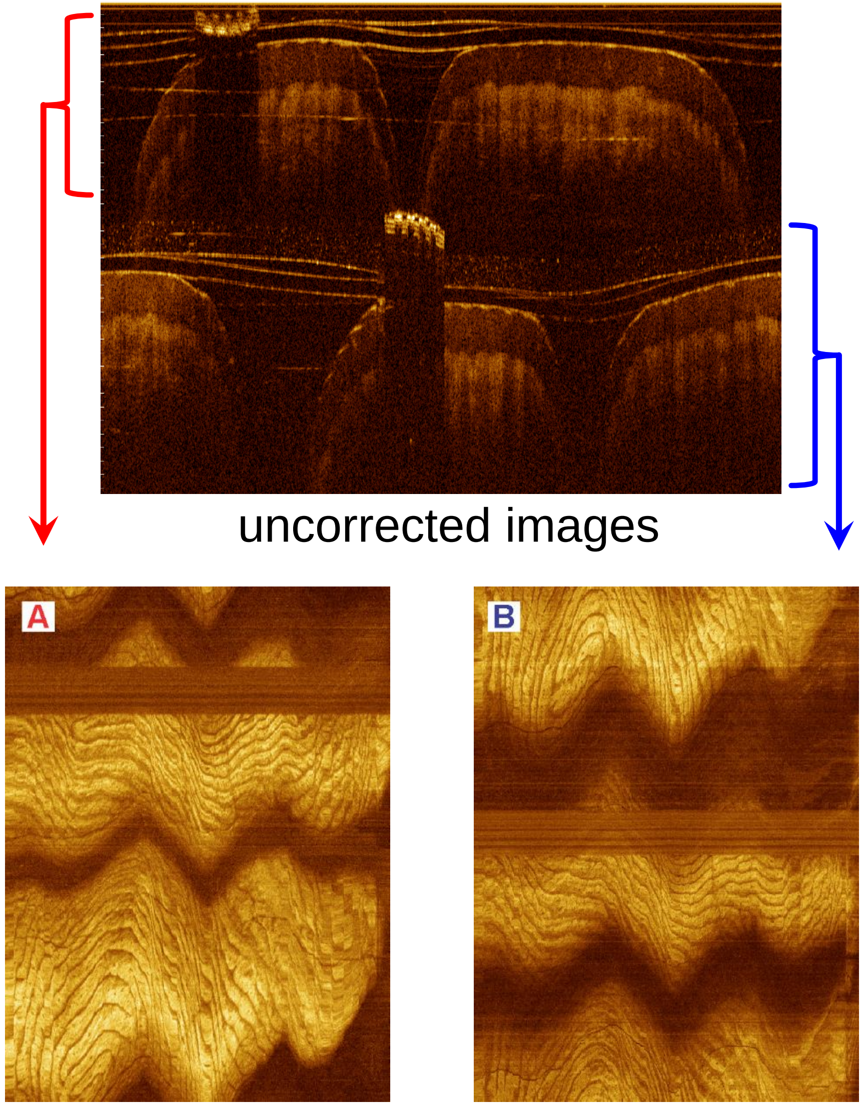

A. Lee (2017)

Appendix III

Additional Material

OCT Image Scanning

- Variations in refractive index → contrast
- **A-scans**
  - Axial scans are 1D signals of backscattered light (magnitude and echo time delay) from a point source
- **B-scans**
  - Transversely scanning in one direction creates a series of A-scans
  - 2D image
- **3D-OCT**
  - Transversely scanning in multiple directions
  - Volumetric data

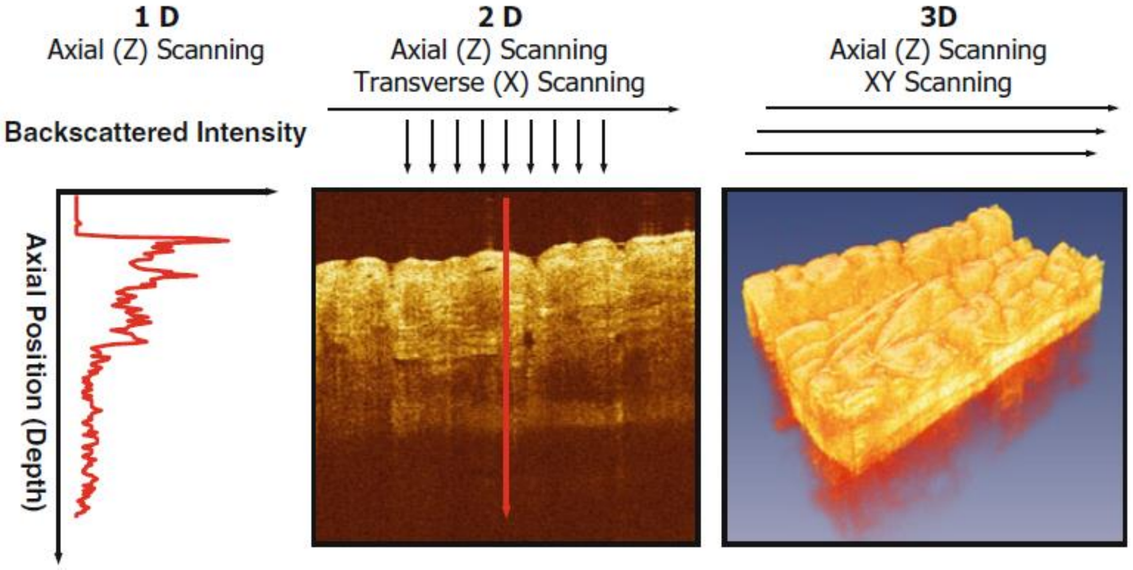

Fig. 1.1 Optical coherence tomography (OCT) generates cross-sectional or three-dimensional images by measuring the magnitude and echo time delay of light. Measurements of backreflection or backscattering versus depth known as axial scans (A-scans). Cross-sectional images are generated by scanning the OCT beam in a transverse direction to acquire a series of axial scans. This generates a two-dimensional data set (B-scan) which can be displayed as a gray scale or false color image. Three-dimensional volumetric data sets (3D-OCT) can be acquired by raster scanning to generate a series of two-dimensional data sets (B-scans)

J.G. Fujimoto, W. Drexler Introduction to OCT Pg. 4

OCT Resolution and Limitations

- OCT fills the gap between Microscopy and Ultrasound
- Axial resolution → bandwidth of light source
  - 1-10 µm
  - 10-1000 times finer than standard ultrasound
- But light is highly scattered and attenuated in tissue
  - Penetration depth ~2mm
- With fiber optics, OCT can be brought into the body to the tissue of interest
  - Endoscopes
  - Catheters

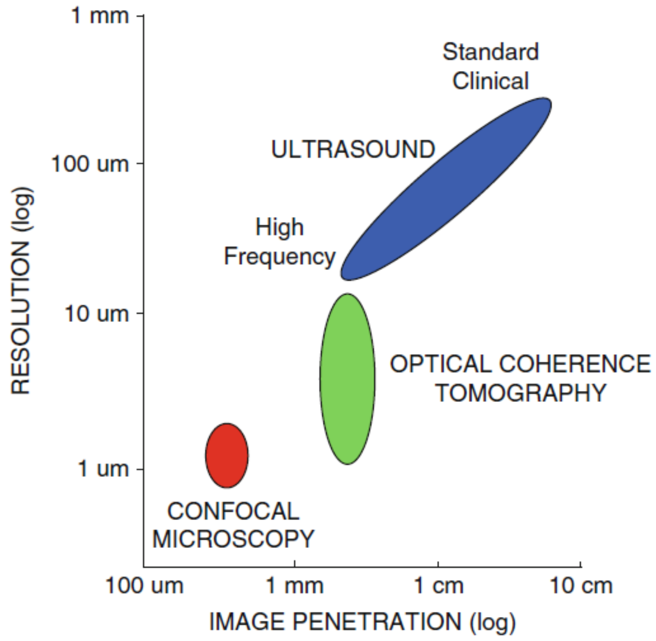

Fig. 1.2 Comparison of ultrasound, OCT, and confocal microscopy resolution and imaging depth. Standard clinical ultrasound achieves deep imaging depths, but has limited resolution. Higher sound frequencies yield finer resolution, but ultrasonic attenuation increases, reducing image penetration. OCT axial image resolution ranges from 1 to 15 µm, determined by the coherence length of the light source. In most biological tissues attenuation from optical scattering limits OCT imaging depth to 2–3 mm. Confocal microscopy has submicron resolution, but imaging depth is only a few hundred microns in most tissues

J.G. Fujimoto, W. Drexler Introduction to OCT Pg. 6

BC CANCER

OCT Detection

- Ultrasound
  - V_sound ~ 1500 m/s
  - Distance resolution ~ 100 µm
  - → Temporal resolution ~ 100 ns ✓
- OCT
  - V_light ~ 3 x10^8 m/s
  - Distance resolution ~ 10 µm
  - → Temporal resolution **~ 30 fs** ✗
- Cannot use direct electronic detection
  - Optical gating
  - Optical correlation
  - Interferometers ✓

Low Coherence Interferometry

- Backscattered light from sample is interfered with a reference path with a known delay
- Classic: Michelson interferometer
  - Incident beam is split into two arms, one to the sample and the other a reference to a mirror at a tunable distance
  - Back-reflected beams amplitudes are combined at the beam splitter using superposition
  - Resultant interference pattern is directed to a detector or camera

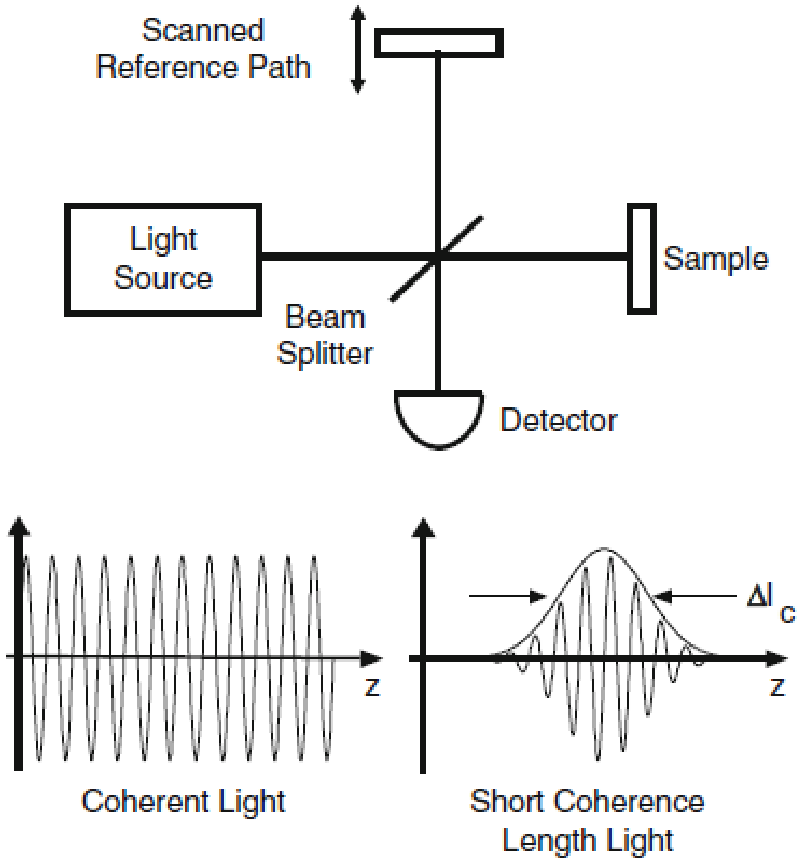

J.G. Fujimoto, W. Drexler Introduction to OCT Pg. 10

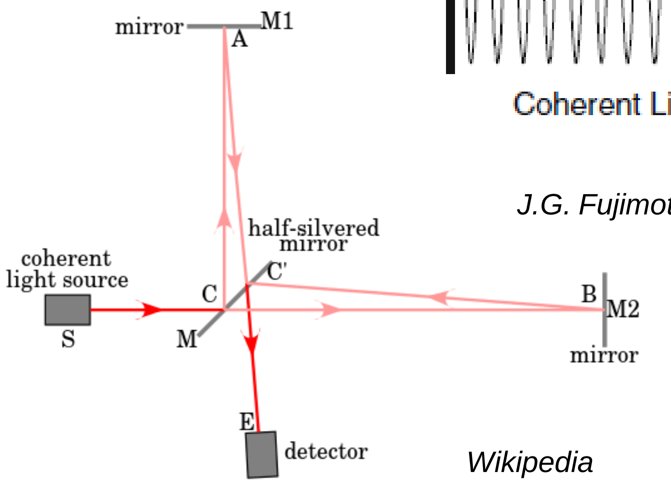

Wikipedia

Interference can only occur when path lengths are matched to within the coherence length

Mach-Zehnder Interferometer

- Used to determine the relative phase shift variations between two collimated beams
- Without a sample, complete destructive interference occurs in the beams reaching detector 2
- With a sample, a change in phase means there is no longer complete destructive interference
- The phase shift produced can be calculated by comparing the relative amount of light entering each detector.

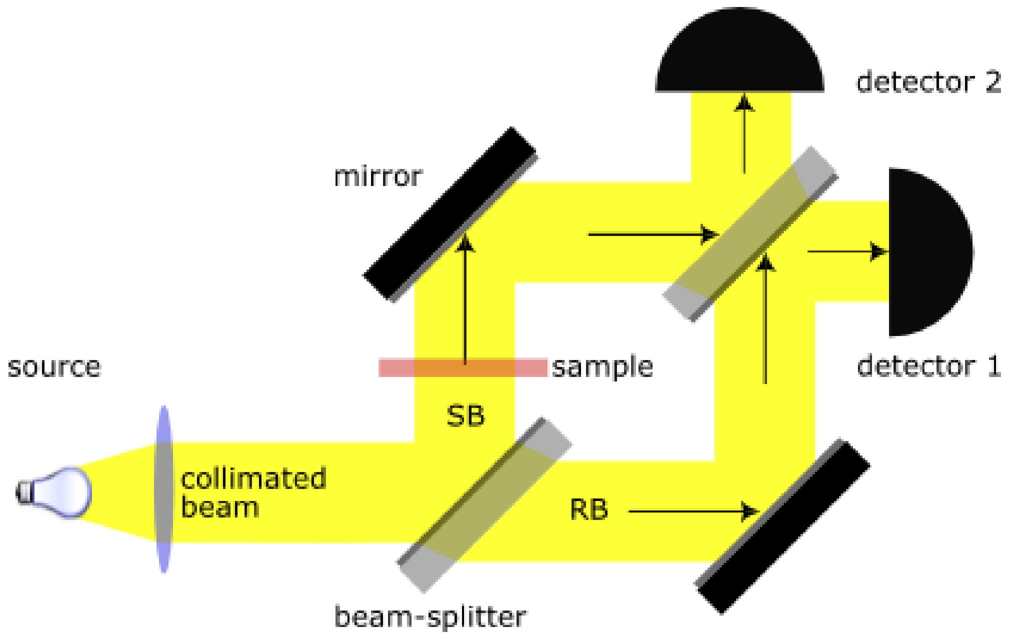

Wikipedia

Time vs. Frequency Domain OCT

- Time Domain
  - Reference arm modulates depth information
  - Mechanically varied reference arm
  - Scan time limited by moving arm

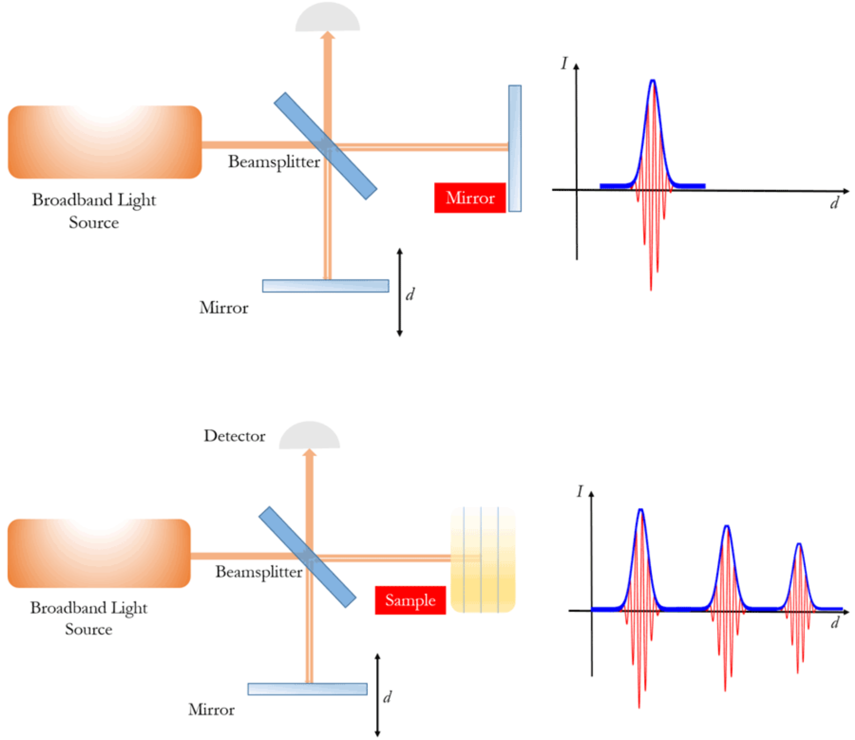

- Frequency Domain
  - Spectrum provides depth information
  - Stationary reference arm
  - Rapidly increased scan time

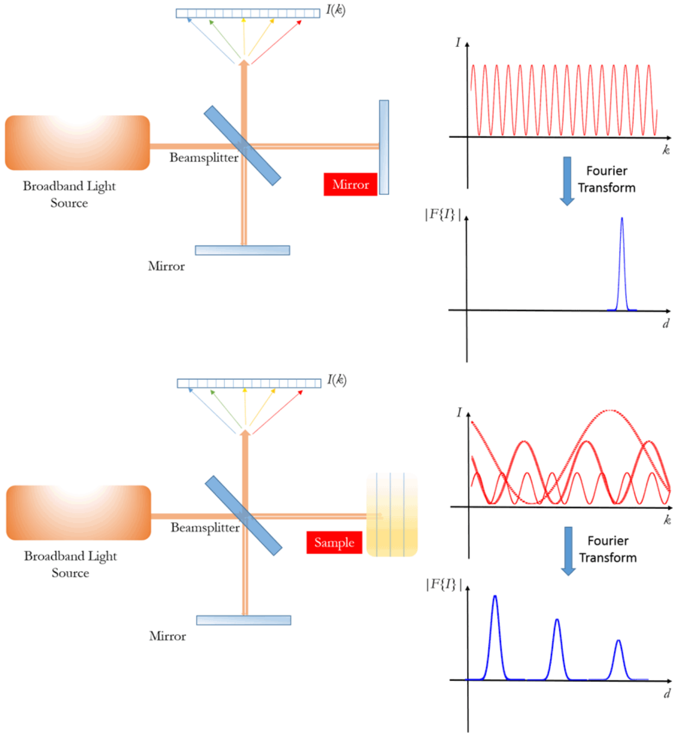

OCT Imaging

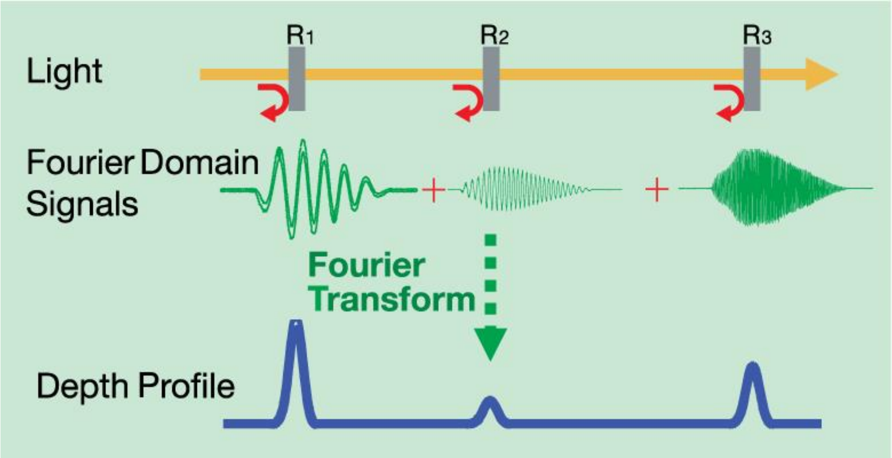
R1
R2
R3
Light
Fourier Domain Signals
Fourier Transform
Depth Profile

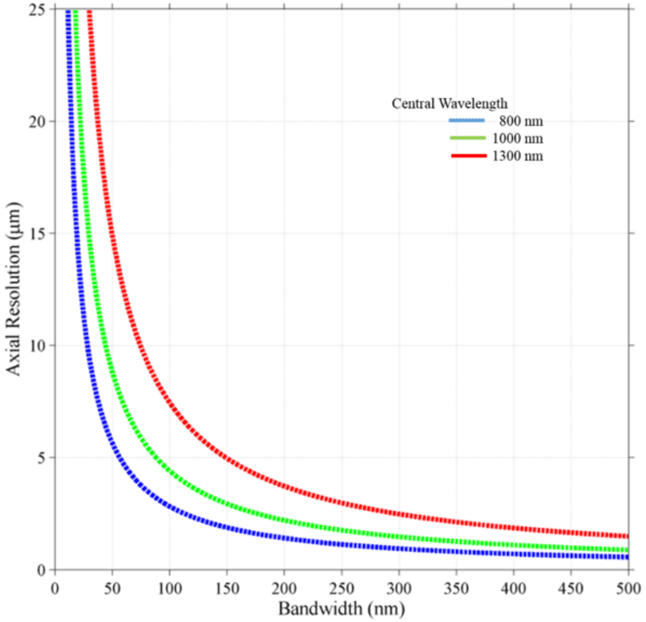
Central Wavelength
800 nm
1000 nm
1300 nm
Axial Resolution (µm)
Bandwidth (nm)
0
5
10
15
20
25
0
50
100
150
200
250
300
350
400
450
500

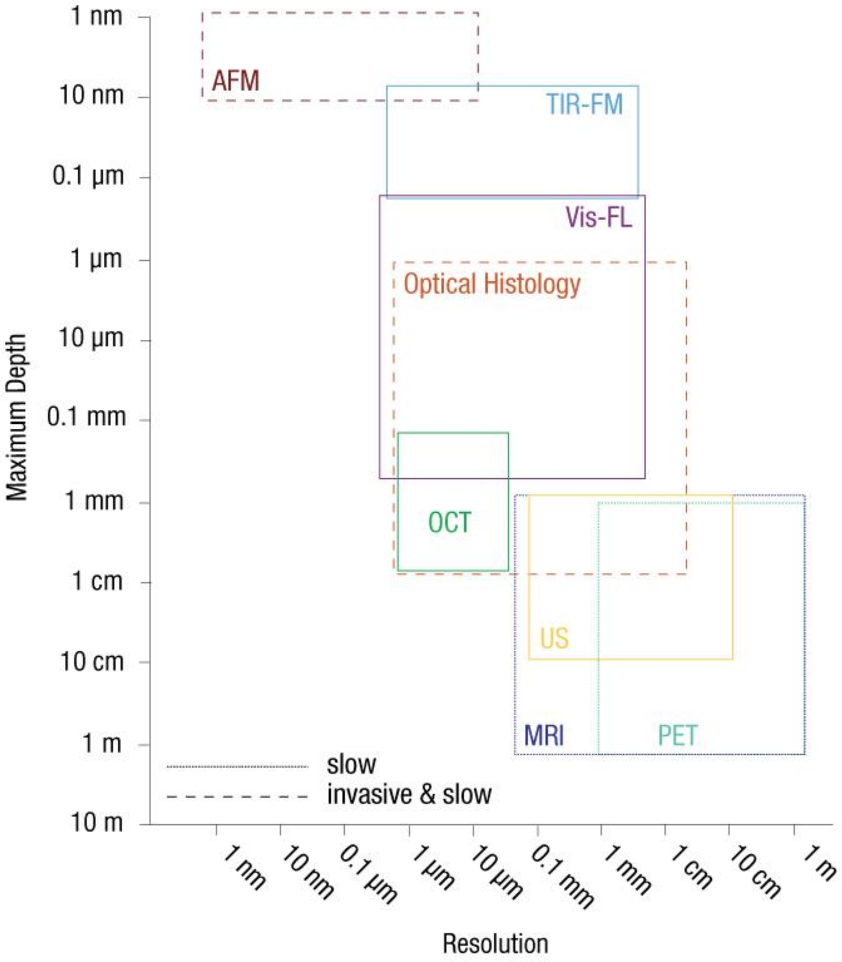
Maximum Depth
1 nm
10 nm
0.1 µm
1 µm
10 µm
0.1 mm
1 mm
1 cm
10 cm
1 m
10 m
AFM
TIR-FM
Vis-FL
Optical Histology
OCT
US
MRI
PET
slow
invasive & slow
Resolution
1 nm
10 nm
0.1 µm
1 µm
10 µm
0.1 mm
1 mm
1 cm
10 cm
1 m

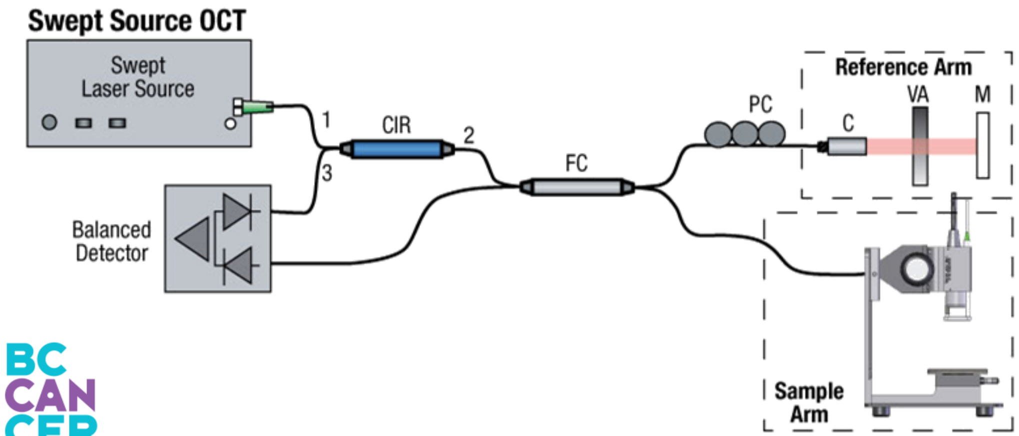
Swept Source OCT
Swept Laser Source
1
2
3
CIR
FC
PC
Reference Arm
C
VA
M
Balanced Detector
Sample Arm

Galvo w/ GRIN Setup

- The GRIN was aligned to the mirror with a 3D printed adapter.
- In the tight constraints, it is difficult to adjust the position and orientation of the GRIN to ensure it is aligned with the center of the mirror
- Also it is impossible to have the beams intersect at the face of the mirror (intersects at face of GRIN)
- Major artefacts in B beam (not due to interferometer, so B portion of the pigtail or position of the B onto the mirror – ie if rotate 180 degrees, does A show same problem?)

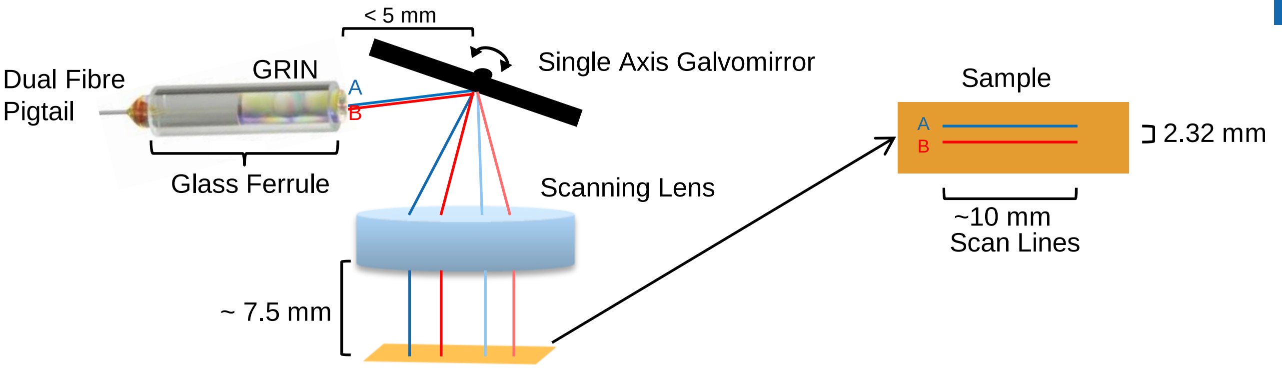

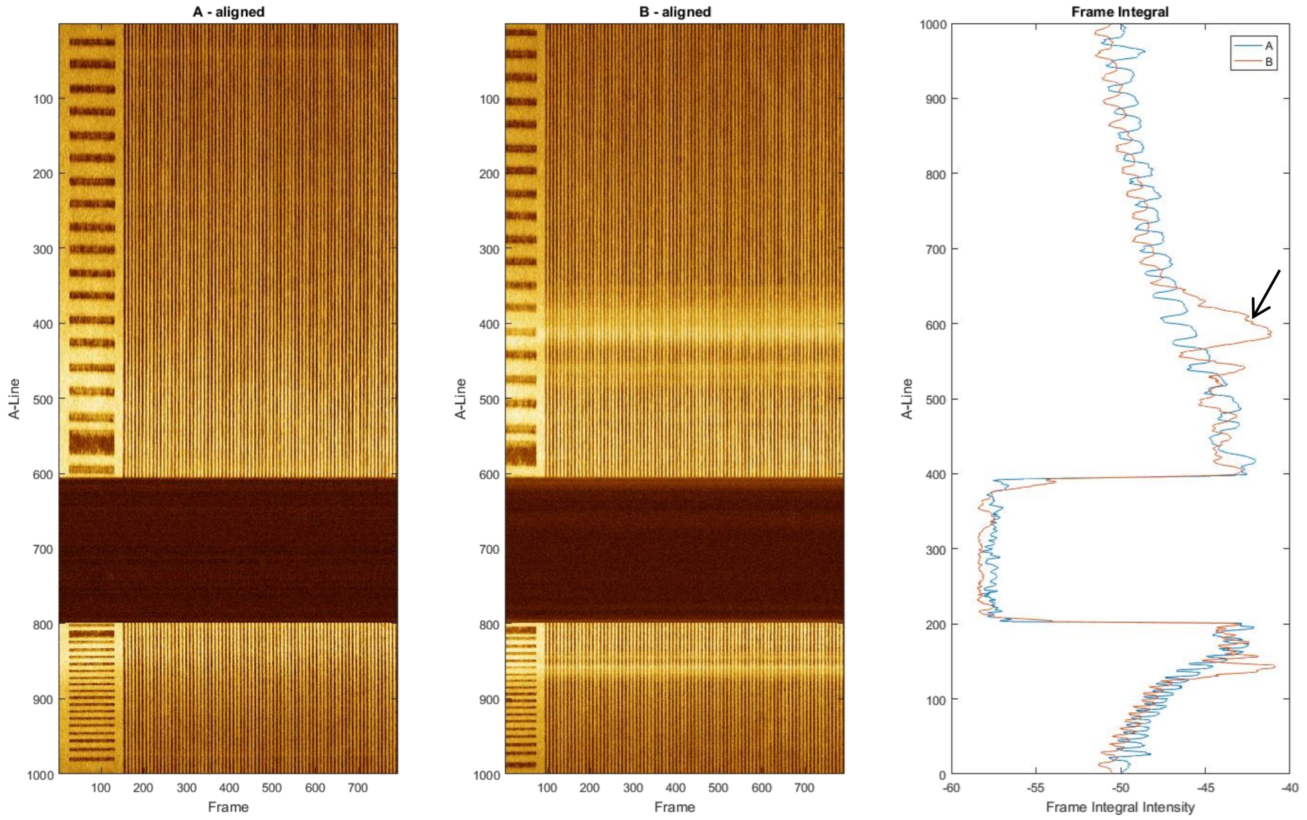

GRIN

- Graded Index Lens – Used as collimator
- Off centre
- Beams cross at the face of the GRIN
- Spot size of ~320-400um

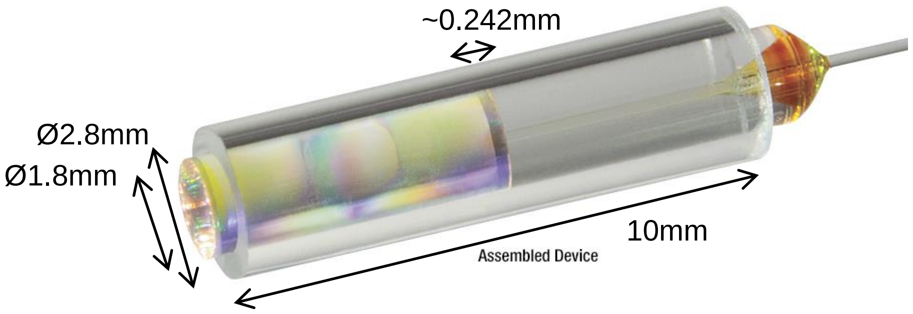

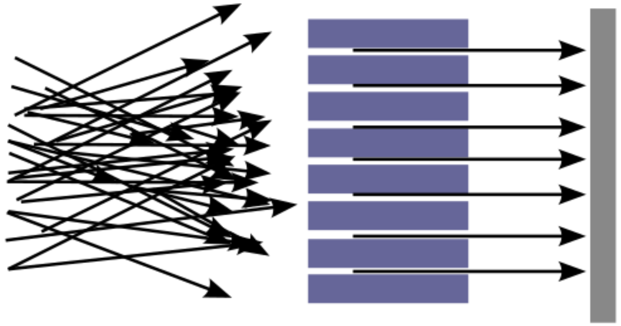

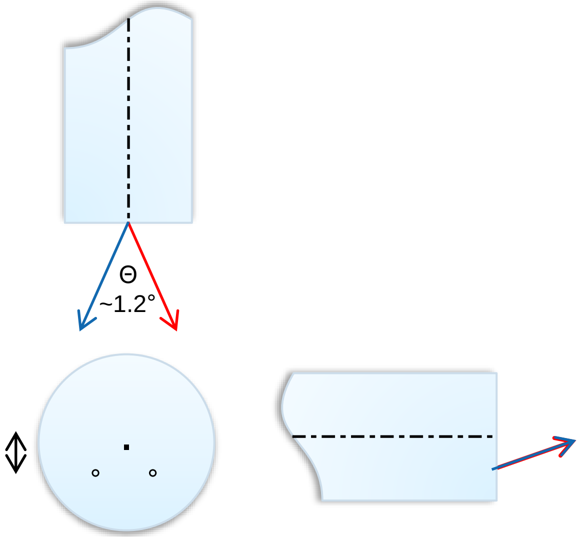

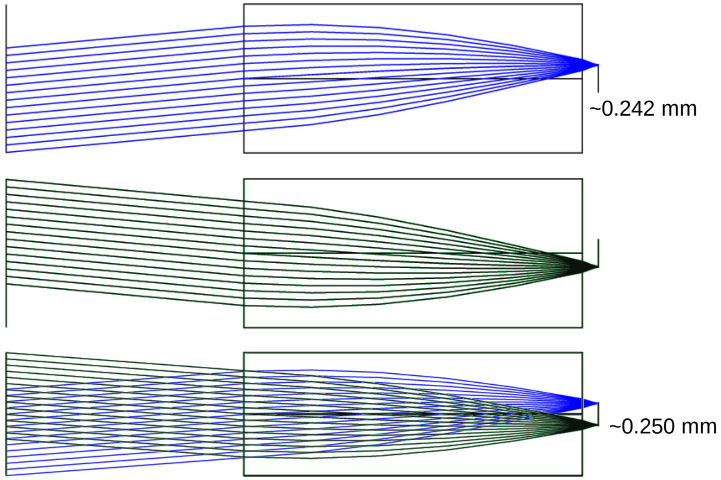

- Marker is used to align a-lines in beams A and B.
- Once N_r is determined in calibration, marker can be used to align and segment image into active and dead zones
- Need unambiguous features in the calibration pattern to identify retrace period and offsets of each beam to the marker.

Swept Source OCT

Swept-Source OCT advantages

- Enables balanced and polarization diverse detection schemes
- Longer Wavelengths, such as 1060 and 1300 nm, enable deeper penetration into tissue
- Increased imaging depth range from slower signal roll-off
- High SNR and Resolution in a compact, rugged package

Highlights:

- High output power (15-18 mW with back trace blanking)
- > 100 nm tuning range (for imaging resolution < 8 μm @1060nm or 15 μm @1310nm
- > 10 mm long coherence length = imaging depth > 5 mm
- 50–100 kHz scan rates for fast data acquisition
- Compact, reliable, and designed for volume manufacturing
- Low noise (RIN < 120dBc/Hz)

	1310 Swept Source
Output Power (Average) (mW)	18
λ Tuning Range (nm)	1250-1360
Sweep Rate (kHz)	50
Coherence Length (Round Trip PL, mm)	13
K-Clock Depth (Std, mm)	5
K-Clock Frequency (MHz)	130
Balanced Detector	Optional
Demonstrated Sensitivity * (dB)	105
Power Supply (vDC)	+12
Size (OEM, mm)	114 x 177 x 58

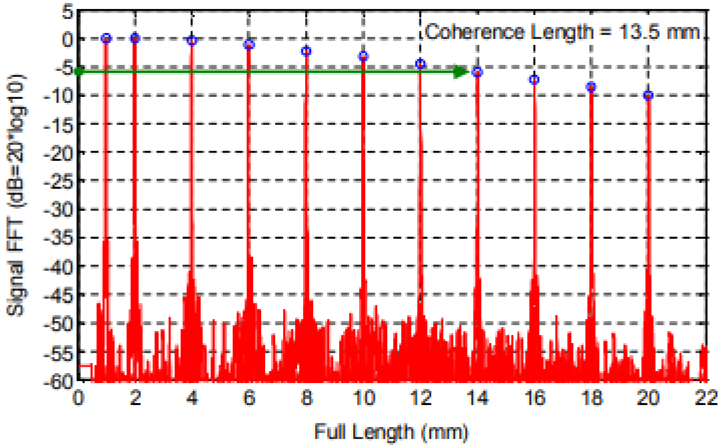

Operating conditions:

- **λ ~ 1060 nm**
- **110 nm** tuning range
- **100 kHz** scan rate

1310nm 50KHz Laser
Power Spectrum from OSA

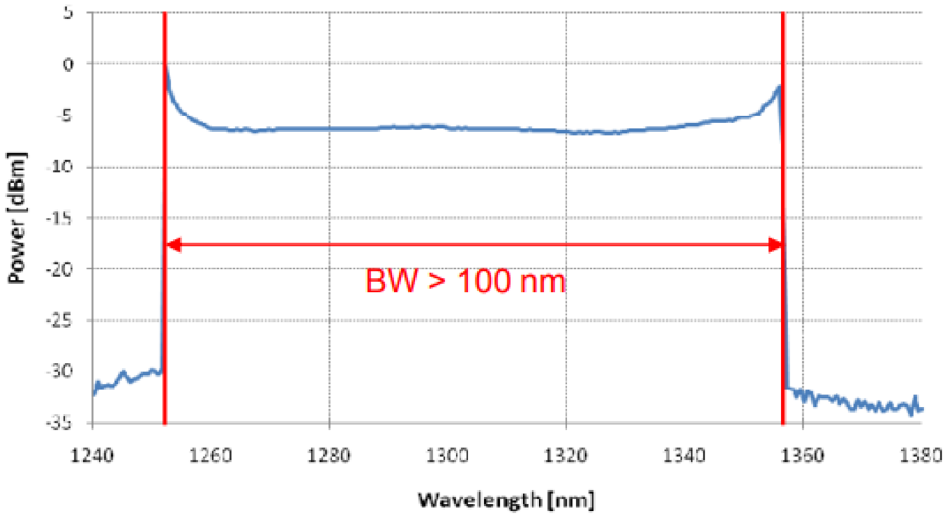

➔ Coherence length **Lc = 13.5 mm**
➔ Corresponds to **55 pm dynamic laser linewidth** FWHM for a Gaussian lineshape

Scanning Lens Specs: LSM 02 - BB

- Telecentric scan lens – optimized for OCT
- Produce a flat image place
- Low f-theta distortion – correct image

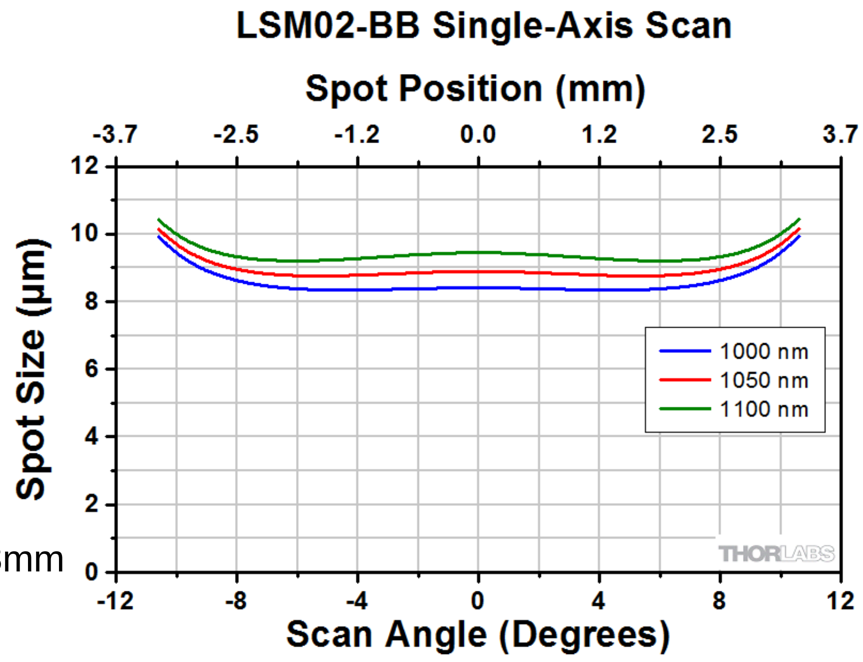

$S = 1.27\lambda * EFL / A$

λ = 1310 nm
S = spot size
A = input beam waist
EFL = Effective focal length = 18mm

Item #		LSM02-BB
Optical Specifications		
Wavelength Range		810 to 890 nm and 1000 to 1100 nm
Effective Focal Length (EFL)		18 mm
Entrance Pupil Diameter[a]		4 mm
Parfocal Distance		30.7 mm
Lens Working Distance		7.5 mm
Scanning Distance[b]		16.1 mm
Optical Scan Angle[c] (Single-Axis Scan)	Maximum	±10.6°
	Diffraction Limited	±10.2° (850 nm) ±10.6° (1050 nm)
Optical Scan Angle[c] (Two-Axis Scan)	Maximum	±7.5° x ±7.5°
	Diffraction Limited	±5.1° x ±5.1° (850 nm) ±5.9° x ±5.9° (1050 nm)
Field of View[d]	Maximum	4.7 x 4.7 mm²
	Diffraction Limited	3.2 x 3.2 mm² (850 nm) 3.7 x 3.7 mm² (1050 nm)
Depth of View[d] (Twice Rayleigh Length)		0.04 mm (850 nm) 0.05 mm (1050 nm)
F-Theta Distortion[d]		<0.9%
Field Curvature[d]		<0.1 mm
Axial Color		5 µm (810 to 890 nm) 10 µm (1000 to 1100 nm)
Lateral Color Shift		5 µm (810 to 890 nm) 5 µm (1000 to 1100 nm)
f/#		4.5
Dimensional Specifications		
Mounting Thread (External)		M25 x 0.75
Thread Length		4.4 mm (0.17")
Barrel Diameter		33 mm (1.30")
Length of Barrel		23.2 mm (0.91")

Galvo Scanner

- Thorlabs GVS012
  - Protected Silver Coating (500nm - 2um range)
  - Max scan angle = +/- 12.5 degrees (0.8V /deg)
  - Position signal +/- 10 V (use only 9.95)
  - Max acceleration 2.

Similarity Measures

- Identity
  - Mean Absolute Difference
  - (not good because our beams may not have the same intensities = not identity)
- Linear
  - Cross Correlation Coefficient
  - (good enough for us)
- Multimodal
  - Mutual Information (Entropy)
  - (would be needed if multimodal)